ALLOYING EFFECTS AND THE g-FACTOR IN ANTIMONY MEASURED BY THE DE HAAS-VAN ALPHEN EFFECT

ALLOYING EFFECTS AND THE g-FACTOR IN ANTIMONY MEASURED BY THE DE HAAS-VAN ALPHEN EFFECT

By

ZAVEN K. ALTOUNIAN, M.Sc.

A Thesis

Submitted to the School of Graduate Studies

in Partial Fulfilment of the Requirements

for the Degree

Doctor of Philosophy

McMaster University

February, 1976

DOCTOR OF PHILOSOPHY (1976) (Physics)

McMASTER UNIVERSITY
Hamilton, Ontario

TITLE: Alloying Effects and the g-factor in Antimony measured by the de Haas-van Alphen Effect

AUTHOR: Zaven Altounian, M.Sc. (The American University in Cairo)

SUPERVISOR: Dr. W. R. Datars

NUMBER OF PAGES: ix,76

SCOPE AND CONTENTS:

The effects of alloying with up to 0.11 atomic per cent tellurium on the Fermi surface of antimony are studied using the de Haas-van Alphen effect. The results are in agreement with the rigid band model predictions. The electron and hole g-factors of antimony are determined from a study of the amplitude and phase of the de Haas-van Alphen oscillations. The experimental g-factors are compared with spin resonance measurements. A theoretical calculation, in the effective mass approximation, permitted an unambiguous determination of the electron g-factors.

ABSTRACT

The dHvA frequencies, cyclotron masses, and Dingle temperatures of antimony-tellurium alloys with up to 0.11 at.% Te were measured using the low frequency field modulation technique. The hole and electron frequencies decreased and increased respectively, as predicted by the rigid band model. At the highest concentration, the increase is about 25% that of pure Sb and the decrease is about 20%. The cyclotron masses of electrons and holes changed with concentration. This dependence resulted from the nonparabolicity of the Sb bands. Estimates of the Fermi surface volume of the alloys indicated that each Te atom contributes one electron to the alloy. The present results are compared with previous dHvA results on antimony-tin alloys.

Antimony g-factors of holes and electrons were also determined by the dHvA effect using the torque and field modulation methods. Possible g-factors were deduced from the harmonic content in the oscillation waveform following the method described by Randles. A measurement of the g-factors at certain field directions was also obtained from spin-splitting of the oscillations observed at high magnetic fields. The excellent agreement between the results of these methods suggests the validity of the Lifshitz-Kosevich equation for antimony and the absence of non-linear effects. The choice of g-factors for electrons from the several possibilities

allowed by the data analysis was determined through a theoretical calculation in the effective mass approximation. These values are consistent with spin resonance and infinite field phase measurements. The choice of hole g-factors was made from a comparison with spin resonance data. The g-factors at the binary, bisectrix and trigonal directions are ∿ 15, 16.8, 3.5 and 4.5, 18.0, 14.5 for the principal branches of electrons and holes, respectively.

ACKNOWLEDGMENTS

I wish to express my thanks to my supervisor, Professor W. R. Datars, for his advice and assistance throughout the course of this work. I also wish to thank Mr. C. A. Verge for the construction of the torque magnetometer and his assistance with many technical problems.

This work was made possible through the financial support of the McMaster University Physics Department and the National Research Council of Canada.

TABLE OF CONTENTS

LIST OF FIGURES

LIST OF TABLES

CHAPTER I

INTRODUCTION

The de Haas-van Alphen (dHvA) effect (a periodic oscillation of the magnetic susceptibility with reciprocal field) has proved to be one of the most powerful and direct experimental methods in the study of the electronic structure of metals and semimetals. dHvA frequency measurements have produced a great deal of precise information on the shapes and sizes of Fermi surfaces. Also, the temperature dependence of the dHvA amplitude gives the cyclotron mass while the field dependence of amplitude gives the Dingle temperature and hence information about electron scattering.

The Landé spin-splitting or the effective g-factor for various materials can now be determined reliably from dHvA measurements due to considerable progress, during the past few years, in the experimental techniques together with a better understanding of the various phenomena involved in these techniques. The value of g can differ from the free electron value of 2.0023 because of spin-orbit coupling (Yafet 1952, 1957) and many-body effects (Landau 1956; Bychkov and Gor'kov 1961). Many-body effects which are manifested in the Coulomb interaction between electrons and the electron-phonon interac-

tion are important in the alkali and noble metals and contribute the most to the difference of the g-factor from the free-electron value in these materials (Randles 1972, Knecht 1975). In semimetals and their compounds, however, the most significant contribution to the g-factor difference comes from the spin-orbit interaction because of the presence of small energy gaps in the vicinity of the Fermi energy. In such materials, where the spin-orbit gaps are of the same order of magnitude as or larger than energy gaps resulting from the crystal potential, the inclusion of spin-orbit effects in an energy band calculation is necessary and the resulting Fermi surfaces from calculations with and without spin-orbit effects differ drastically. Experimental g-factor measurements provide valuable information about the importance and magnitude of these effects and contribute to the further understanding of the quantum theory of metals. In antimony, the g-factor is expected to be significantly larger than the free electron value because the spin-orbit coupling is large compared to the band gap (Luttinger 1956). This is true for all group V semimetals and their compounds. Previous g-factor measurements in antimony were confined to spin-splitting zero directions of dHvA oscillations (Windmiller 1966) and to direct observations of spin-splittings in the magnetothermal oscillations from electrons for magnetic field directions in the bisectrix-binary plane and from holes with the magnetic field parallel to the bisectrix axis (McCombe and

Seidel 1967).

The investigation of the effect of impurities on the dHvA effect in a metal also yields valuable information on the corresponding changes in the Fermi surface, the band shapes or the rigidity of the bands, and the electron energy dispersion law. For dilute alloys, the rigid band theory states that the band structure remains unchanged and the Fermi level is lowered or raised according to the concentration and type of carriers added. Studies of the effect of alloying on the Fermi surface of bismuth (Bi(Te), Weiner (1962), Bi(Sb), Kao (1964), and Bi(Pb), Bhargava (1967)) support the validity of the rigid band model. More recent studies on a number of dilute alloys of copper (Coleridge and Templeton 1971) indicate that the dHvA frequency shifts do not necessarily agree with the rigid band prediction. The present alloy work is an extension of an earlier study (Dunsworth and Datars 1973) of antimony-tin alloys. Antimony is a semimetal which has the A7 crystal structure that is similar to bismuth and arsenic. Due to the small overlap between the fifth and sixth bands, an equal number of electrons and holes coexist. The addition of tin to antimony caused the Fermi surface of holes and electrons to increase and decrease, respectively. The frequency shifts observed on alloying were described well by the rigid band predictions except for the hole surface at high concentrations. The results also indicated non parabolic

conduction and valence bands. In our present system of antimony-tellurium alloys, the addition of Te increases and decreases the electron and hole surfaces respectively because Te has one more valence electron than Sb. The comparison of present results with the previous Sb(Sn) results permits a rigorous test of the rigid band model for Sb alloys because rigid bands are postulated to be independent of the type of solute atoms. The first investigation of the dHvA effect in the Sb(Te) system was reported by Ishizawa (1968) for a nominal concentration of 0.20 at. % Te. The final concentration of Te in the alloy was not determined, but the resulting changes in the Fermi surface enabled a conclusive assignment of the dHvA frequency branches to electrons and holes.

Detailed results of g-factor measurements in antimony and the dHvA effect in Te doped antimony will be presented and discussed in this study. A brief theoretical background of the dHvA effect is given in Chapter II. In Chapter IV, the experimental methods are discussed. These include experimental procedure, crystal growth and dHvA signal detection techniques. The experimental results are presented in Chapter V, while Chapters VI and VII present a discussion of the alloys and g-factor results respectively. Chapter VIII consists of summary and conclusions of the study.

CHAPTER II

THEORY OF THE dHvA EFFECT

The de Haas-van Alphen (dHvA) effect is the phenomenon of the oscillatory dependence on magnetic field of the magnetic properties of a metal single crystal at sufficiently low temperatures. The effect was first observed in Bi by de Haas and van Alphen, in 1930. This oscillatory behaviour is a direct consequence of the quantization of the motion of the conduction electrons or holes in a magnetic field. In the absence of a field, the electrons have a continuous range of energies up to the Fermi energy E_F. When a magnetic field $\bar{H}$ is applied in the z-direction, k_z remains unquantized but for a given k_z, only certain discrete energy levels, E_n, called the Landau levels, are available. The separation between these Landau levels increases with H. For a given k_z, the quantized values of the energy corresponding to the allowed areas, A_n, in k-space are given by the Onsager relation (Onsager 1952)

$$A_n = 2\pi(n+\gamma)\frac{eH}{\hbar} \qquad [II-1]$$

where n is an integer, and γ is a constant depending on the form of the electronic structure. For quadratic dispersion laws $\gamma = 1/2$. Each allowed orbit is highly degenerate, and

can accomodate all the electrons which would, in zero field, lie between it and the next allowed orbit. As the magnetic field H is increased the Landau levels are drawn up in energy so that the total free energy increases to a maximum when a Landau level is at the Fermi energy. But when this level passes through the Fermi level it begins to empty and the average energy of the electrons drops, reaching a minimum when the Fermi level lies halfway between two Landau levels. Thus, the free energy of the electrons oscillates about its zero-field value as the magnetic field H increases or decreases.

The full expression of the oscillatory part of the free energy of a metal under a magnetic field H, and at temperature T, is given by the Lifshitz-Kosevich (LK) equation (Lifshitz and Kosevich 1955)

$$\Phi_{osc} = \sum_i \Phi_{osc}^{(i)} = 2Vk_B\left(\frac{e}{2\pi\hbar}\right)^{\frac{3}{2}} TH^{\frac{3}{2}} \sum_i \left|\frac{\partial^2 A_i}{\partial k_z^2}\right|_{ext}^{-\frac{1}{2}} \sum_{r=1}^{\infty} \frac{e^{-r\alpha m_i^* T_D/H}}{r^{3/2}\sinh(r\alpha m_i^* T/H)}$$

$$\times \cos\left(\frac{r\pi g}{2} m_i^*\right)\cos\left(2\pi r \frac{F_i}{H} - 2\pi r\gamma \mp \frac{\pi}{4}\right) \quad [II-2]$$

where the subscript i denotes the various possible extremal areas. r is the harmonic number, m^* is the cyclotron mass (in units of the free electron mass, m_o) given by

$$m^* = \frac{1}{m_o}\frac{\hbar^2}{2\pi}\frac{\partial A}{\partial E} . \quad [II-3]$$

The constant $\alpha = \frac{2\pi^2 m_o k_B}{e\hbar} = 14.69$ Tesla/K, V is the volume of the crystal and k_B, e, $\hbar$ have their usual values.

F is the dHvA frequency and is related to the extremal cross-sectional area A by

$$F = \frac{\hbar}{2\pi e} A. \qquad [II-4]$$

The $\mp$ signs in the expression for the dHvA phase apply according as A represents a maximum (-) or a minimum (+). T_D is the Dingle temperature which takes account of the broadening of the Landau levels on account of the finite lifetimes of states due to various scattering mechanisms. If the broadening is due only to collisions then

$$T_D = \frac{\hbar}{2\pi k_B} \frac{1}{\tau} \qquad [II-5]$$

where τ is the scattering time.

$\left|\frac{\partial^2 A_i}{\partial k_z^2}\right|_{ext.}$ is the geometric curvature factor of the Fermi surface evaluated at the extremum.

The factor $\cos\left(\frac{\pi r g m^*}{2}\right)$ arises from the lifting of the spin degeneracy by the magnetic field. The spin moment will interact with the magnetic field to produce in general a symmetric Zeeman splitting of each Landau level by the amount $g\mu_B H$ where μ_B is the Bohr magneton, and g is the effective g-factor. Thus there are two sets of levels with the same spacing but shifted in phase by $2\pi(\frac{gm^*}{2})$. The oscillatory

free energy of both sets will then add coherently giving the factor $\cos\left(\frac{\pi r}{2}\, gm^*\right)$.

The oscillatory magnetization per unit volume parallel to $\bar{H}$ can be found by differentiating [II-2] with respect to H.

$$M_i = \frac{1}{V}\left(\frac{\partial \phi^i}{\partial H}\right)_{T,V}$$

$$= -\lambda \frac{F_i T}{H^{1/2}} \left|\frac{\partial^2 A_i}{\partial k_z^2}\right|_{ext}^{-1/2} \sum_{r=1}^{\infty} \frac{e^{-\alpha r m^* T_D/H}}{r^{1/2}\sinh(\alpha r m^* T/H)} \cos(\pi r S) \sin\left(2\pi r \frac{F_i}{H} - 2\pi r\gamma \mp \frac{\pi}{4}\right) \qquad [II-6]$$

where $S = \frac{1}{2} m^* g$ and the constant

$$\lambda = \frac{2k_B}{\sqrt{2\pi}} \left(\frac{e}{\hbar}\right)^{3/2} = 6.516\ 10^{-6}\ G^{1/2}/K\ .$$

It should be noted that in obtaining the expression of the oscillating magnetization only the cosine terms involving the dHvA phase were considered in performing the differentiation since their variations with the field are much more rapid than those of the other field-dependent factors in the dHvA amplitude.

CHAPTER III

FERMI SURFACE OF ANTIMONY

All group V semimetals, including antimony, crystallize into a lattice with rhombohedral symmetry of the A7 classification. The rhombohedral primitive cell is closely related to the fcc lattice. The Brillouin zone of the A7 structure is shown in Fig. 1. This resembles the fcc Brillouin zone but compressed along ΓT, the cube body diagonal. This distortion from a cubic structure reduces the symmetry elements to the trigonal axis ΓT, the three binary axes, ΓK perpendicular to ΓT, and the three mirror planes σ passing through ΓT. In these mirrors, rotations from the trigonal axis ΓT by equal amounts but in opposite directions are not equivalent.

With two atoms per unit cell and five valence electrons per atom, antimony has a sufficient number of valence electrons to completely fill five bands. However, due to a small overlap between the fifth and sixth energy bands an equal number of holes and electrons are formed in small, nearly ellipsoidal pockets, giving rise to semimetallic behaviour. The pockets for each carrier are located at equivalent points of the Brillouin zone so they transform among themselves under the symmetry operations of the reciprocal lattice.

Extensive experimental Fermi surface studies of pure

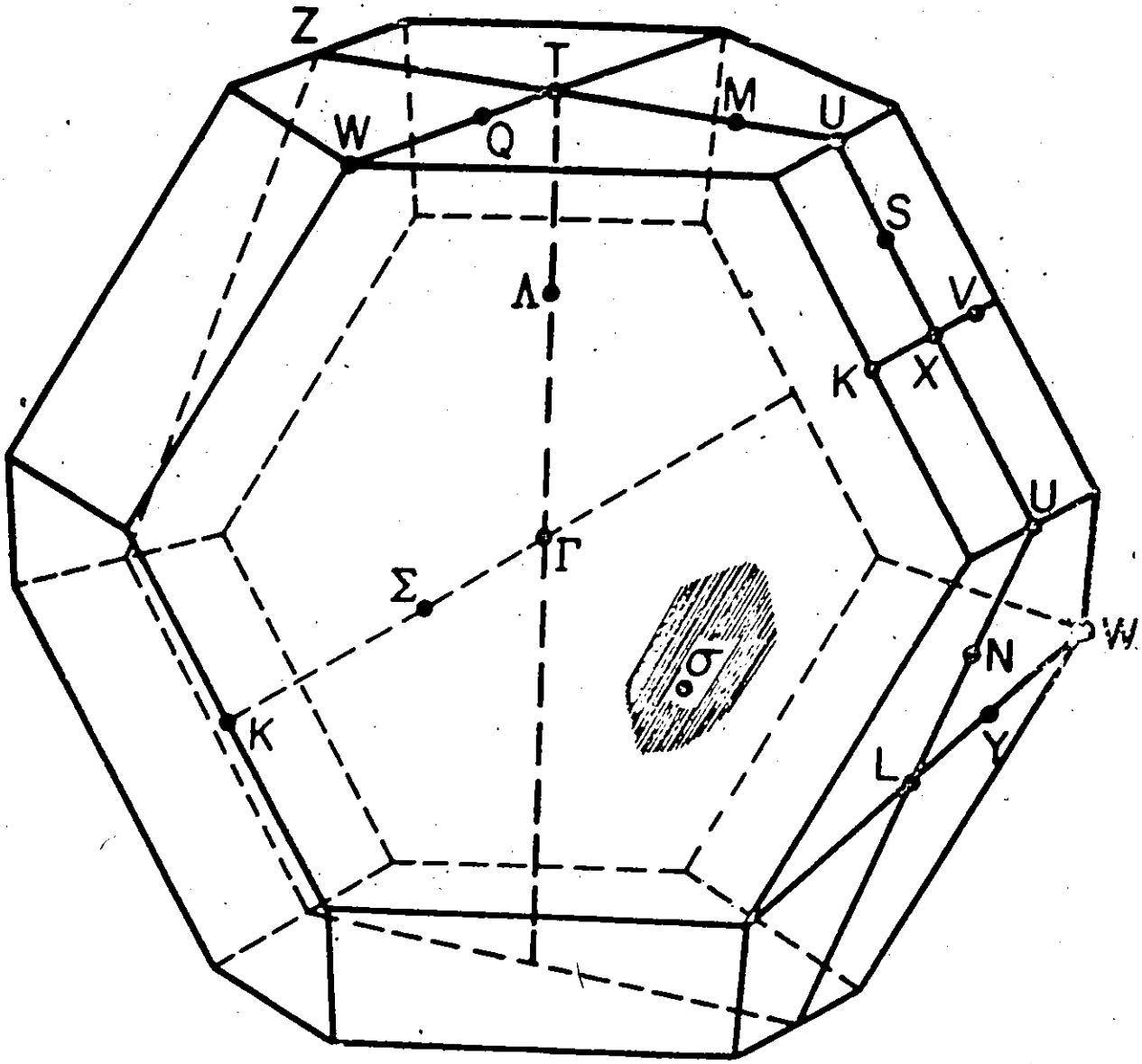

Fig. 1 The Brillouin zone of the A7 structure, showing the points, lines and planes of symmetry.

antimony (Nanney (1963), Datars and Vanderkooy (1964), Windmiller (1966), Tanaka et al. (1968), Herod et al. (1971)) together with the pseudopotential band structure calculations of Falicov and Lin (1966) show that the electrons are located in three equivalent pockets centered at the points L of the Brillouin zone, thus possessing a center of inversion, while the holes are located in six equivalent pockets centered at points on the mirror plane σ near T. The pockets are roughly ellipsoidal with deviations that can be measured experimentally.

The right handed cartesian coordinate system is conventionally used to represent the data. The z-axis is chosen parallel to the trigonal axis, the x-axis is chosen parallel to a binary axis, and the y-axis is chosen parallel to the bisectrix of the other two binary axes. Thus each set of carriers, for example, will generate two extremum cross-sectional areas (dHvA frequency branches) in the trigonal-bisectrix plane, a principal branch associated with the principal pockets having either 2-fold symmetry about the binary axis, mirror symmetry, or both and two non-principal branches associated with the pockets generated from the principal ones by rotations of $\pm 120°$ about the trigonal axis.

CHAPTER IV

EXPERIMENTAL METHODS

1. MATERIALS

Antimony samples for g-factor and absolute phase measurements were prepared from 99.9999% pure Sb. The Sb crystals were spark cut into cubes with a side dimension of 0.2 cm for the field-modulation technique and 0.4 cm for use with the torque magnetometer. The crystals were handled with extreme care in all phases of sample preparation. Extensive x-ray photographs were taken to ensure that the samples used were strain-free single crystals.

The alloys were prepared from 99.9999% pure Sb and Te following the method used to grow Sb(Sn) alloys (Dunsworth and Datars 1973). The appropriate amounts of Sb and Te were placed in a carbon coated vycor tube. The carbon coating prevented the alloy from sticking to the tube after melting. To prevent evaporation, the tube was evacuated and filled with argon. Single crystals were grown using a horizontal reverse multipass zone melting technique.

The distribution constant k_o, defined as the ratio of the concentration of tellurium in the solid to the concentration of tellurium in the liquid, is 0.025 as determined from the phase diagram. The effective distribution constant k_{eff} was calculated to be 0.09 for experimental growth conditions. Due to the relatively low value of k_{eff}, it was found, using

the equations of Braun and Wang (1961), that seven passes were enough to give a uniform tellurium concentration in the alloy except at the last molten zone. The alloys were annealed at about 600°C for 1 week under an argon atmosphere to further homogenize the tellurium concentration. The samples were spark cut from the ingot into cubes of about 2 mm per side. The samples were oriented by back reflection Laue photographs.

If C_o is the nominal concentration of Te, and C_f is the final uniform concentration, then (Pfann 1966)

$$C_f = C_o/\{1 + \frac{\ell}{L}\,(\frac{1}{k_{eff}} - 1)\} \qquad [IV-1]$$

where L is the total length of the ingot, and ℓ is the length of the molten zone. For the experimental conditions $\ell = 2$ cm for all samples and L = 12 cm for samples 1 and 2, and L = 10 cm for samples 3 and 4 respectively.

The exact Te content was determined by atomic absorption spectroscopy. The results from atomic absorption together with the predicted concentrations of Te from [IV-1] are tabulated in Table 1 . The agreement is very good. Attempts were made to prepare samples with higher concentrations of Te but it was found that not all the Te went into the solid solution, because of the low solid solubility limit of Te in Sb (Abrikosov et al. (1959).

Table 1. Tellurium concentrations of samples studied

Sample No.	Nominal Te conc. (wt. %)	C_f (wt. %) from [IV-1]	Te conc. (wt. %) atomic absorption	Te conc. (at. %) atomic absorption
1	0.15	0.056	0.057	0.054
2	0.20	0.074	0.074	0.071
3	0.30	0.099	0.099	0.095
4	0.35	0.116	0.114	0.110

2. EXPERIMENTAL TECHNIQUES

The dHvA measurements were done with the samples in a 55 kOe Westinghouse superconducting magnet at a sample temperature range between 1.1 and 4.2 K. The dHvA oscillations were detected for the alloy studies by the low-frequency field-modulation technique using apparatus described previously (Poulsen et al. (1971)). The modulation frequency of 517 Hz that was used was low enough for complete penetration of the modulation field into the sample because of the high magnetoresistance of Sb. All the dHvA frequencies were detected at the second harmonic of the modulating frequency. The temperature was determined by measuring the liquid ^{4}He vapour pressure above the sample space with a Texas Instruments precision gauge. The data were collected on magnetic tapes and Fourier analysed by computer. The dHvA amplitude at the desired frequency was calculated from the sine and cosine

Fourier components of that frequency. The cyclotron mass was calculated from the temperature dependence of the dHvA amplitude at constant field. The Dingle temperature was found from the field variation of the dHvA amplitude at constant temperature.

In the field modulation technique, a small oscillating magnetic field $h = h_o \cos\omega t$ is applied parallel to the large d.c. field H_o, where $\omega/2\pi$ is the modulation frequency. The total field $H = H_o + h_o \cos\omega t$. The first term of [II-6] then becomes

$$M_i = A_i(H_o,T)\sin\left(\frac{2\pi F_i}{H_o + h_o\cos\omega t} - 2\pi\gamma \mp \frac{\pi}{4}\right) \qquad [IV-2]$$

where $A_i(H_o,T)$ includes all the other field and temperature dependent functions of [II-6]. The expression [IV-2] for the magnetization, as $h_o << H_o$, can be expanded to give

$$M_i = A_i(H_o,T)\left[\sin\left(\frac{2\pi F_i}{H_o} - 2\pi\gamma \mp \pi/4\right)\cos(a\cos\omega t) - \cos\left(\frac{2\pi F_i}{H_o} - 2\pi\gamma \mp \pi/4\right) \times \sin(a\cos\omega t)\right] \qquad [IV-3]$$

where $a = \dfrac{2\pi F_i h_o}{H_o^2}$.

Equation [IV-3] can be further expanded into its harmonic components in terms of Bessel functions (Goldstein et al. 1965). For second harmonic detection, $\frac{dM_i}{dt}$ which is proportional to the dHvA signal detected is given by

$$\left(\frac{dM_i}{dt}\right) = 4\omega A_i(H_o,T)J_2(a)\sin\left(\frac{2\pi F_i}{H_o} - 2\pi\gamma \mp \pi/4 + \pi\right). \qquad [IV-4]$$

To obtain an expression for field and temperature dependent terms of the dHvA amplitudes, each term in [II-6] should be multiplied by its corresponding second order Bessel function, $J_2(\frac{2\pi r F_i h_o}{H_o^2})$.

For the g-factor measurements, the dHvA effects were also detected using a torque magnetometer in addition to the field-modulation technique. The torque method is an ideal method for studying low dHvA frequencies. The oscillatory torque, as measured by the torque magnetometer, is obtained by differentiating the free energy as given by [II-2] with respect to θ, the angular variable in the plane normal to the axis about which the torque is measured. The result is

$$\tau_i = (\frac{\partial \Phi_i}{\partial \theta})_H = -\lambda F_i T\sqrt{H}\ \frac{\partial F_i}{\partial \theta}\left|\frac{\partial^2 F_i}{\partial k_H^2}\right|_{ext}^{-1/2} \sum_{r=1}^{\infty} \frac{e^{-r\alpha m^* T_D/H}}{r^{1/2}\sinh(r\alpha m^* T/H)}$$

$$\times \cos(\frac{r\pi g m^*}{2})\sin(\frac{2\pi r F_i}{H} - 2\pi r\gamma \mp \pi/4) \qquad [IV-5]$$

Equivalently as $\bar{\tau} = \bar{M}\times\bar{H}$, the torque on a sample in a magnetic field measures the component of magnetization perpendicular to both the field direction and the axis of suspension of the sample.

$$M_\perp = -\frac{\lambda F_i T}{\sqrt{H}}\left|\frac{\partial^2 A_i}{\partial k_H^2}\right|_{ext}^{-1/2} \frac{\partial F_i}{\partial \theta} \sum_{r=1}^{\infty} \frac{e^{-r\alpha m^* T_D/H}\cos(\frac{r\pi g m^*}{2})}{r^{1/2}\sinh(r\alpha m^* T/H)}$$

$$\times \sin(\frac{2\pi r F_i}{H} - 2\pi r\gamma \mp \pi/4)\ . \qquad [IV-6]$$

It is clear that the torque or the perpendicular component of the magnetization vanishes at symmetry and frequency extrema directions where $\frac{\partial F_i}{\partial \theta} = 0$.

The torque magnetometer used in the measurements was constructed by C. Verge. A block diagram is shown in Figure 2. The self-balancing torque magnetometer differs from conventional magnetometer design in that the pick-up coil is stationary and parallel to the superconducting magnet whereas the modulating coils necessary for position control and orientation are a pair of mutually perpendicular rotating coils with the sample located in the centre. This arrangement has the advantage that it permits dHvA measurements in an angular variation of $\theta = \pm 100°$ in any desired plane. The torque on the sample or the normal component of the magnetization is detected as an error voltage required in a feedback process to balance the torque. In this feedback process, the error signal is divided by the magnitude of the field H and multiplied by $\sin\theta$ and $\cos\theta$ for the two modulation coils respectively. This process insures that the sensitivity and the compliance factor of the torque magnetometer are constant for all angular positions and magnetic fields. All torque data were taken by sweeping the magnetic field at fixed angular positions. However due to its versatility the present magnetometer can also be used as a vibrating sample magnetometer in both sweeping field at fixed orientation or during crystal rotation at fixed field.

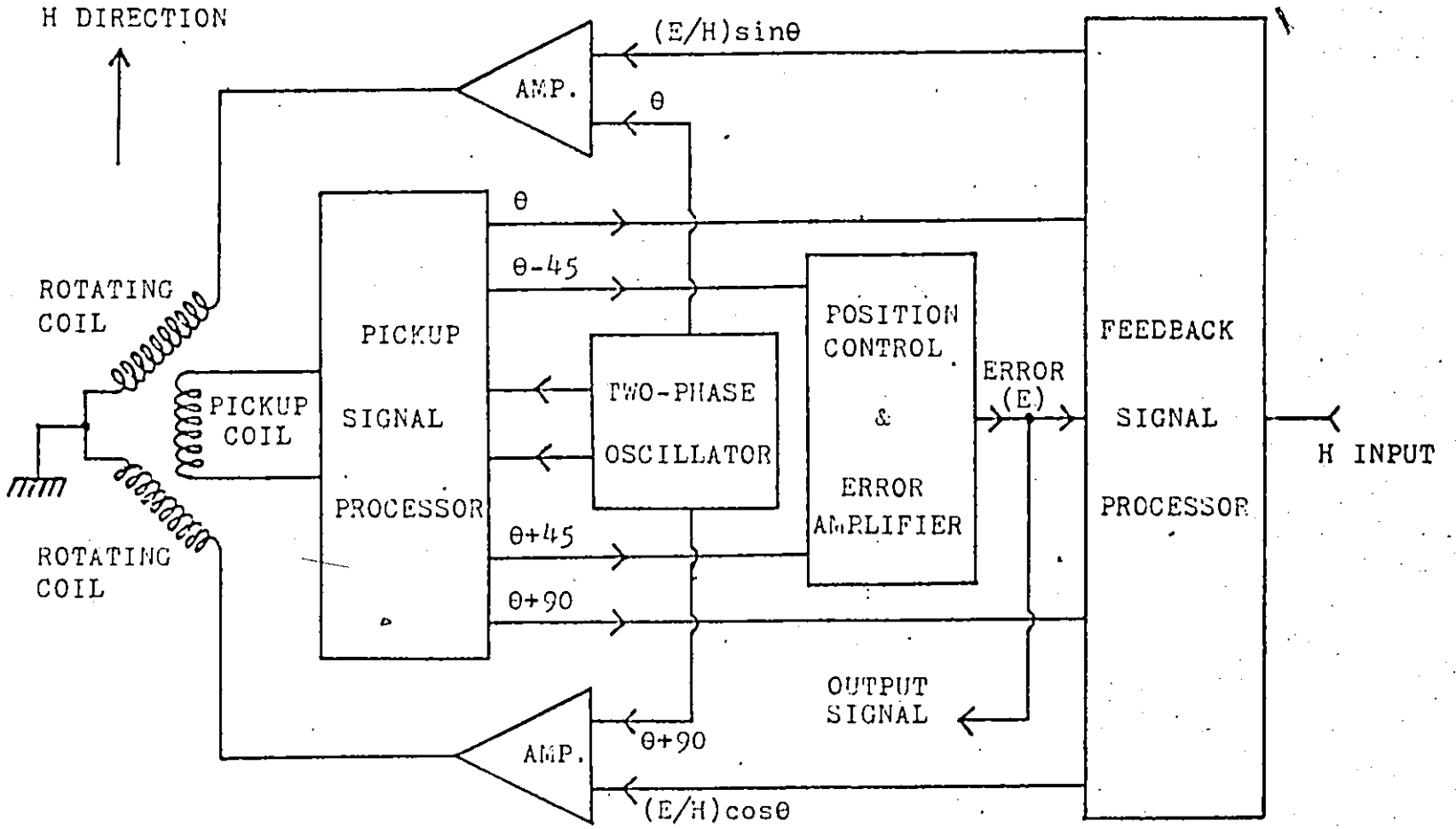

Fig. 2 Block diagram of the torque magnetometer

3. PROCEDURE FOR DETERMINING g-FACTORS

In principle, the simplest method for determining the g-factor is to measure the absolute amplitude of the dHvA fundamental frequency. Experimentally this is the most difficult method because it requires a knowledge of the cyclotron mass, the Dingle temperature, the curvature factor and a reliable calibration of the detection apparatus. This method can only be applied to materials having a simple dHvA frequency spectrum and a nearly spherical Fermi surface that gives reliable and accurate curvature factors. In fact this method of absolute amplitude has only been applied successfully to the alkali metals (Randles 1972, Knecht 1975).

In order to avoid these limitations, the g-factors are extracted from the harmonic content in the oscillation waveform. This method was suggested by Shoenberg and Vuillemin (1966) and applied to the noble metals by Randles (1972) and Alles et al (1975). In this method the ratio of the dHvA fundamental amplitude to the second harmonic is measured. From [II-6] this ratio is

$$\frac{A_1}{A_2} = \sqrt{2}\, e^{\alpha m^* T_D/H} \frac{\sinh(2\alpha m^* T/H)}{\sinh(\alpha m^* T/H)}\, G \qquad [IV-7]$$

where $G = \cos(\pi S)/\cos(2\pi S)$. In the field modulation experiments the right hand side of [IV-7] also includes the factor $J_2(2\pi F h_o/H_o^2)/J_2(4\pi F h_o/H_o^2)$. Knowing m^* and T_D, the quantity G can be calculated without a knowledge of curvature factors and the calibration of the detection system. Figure 3 shows

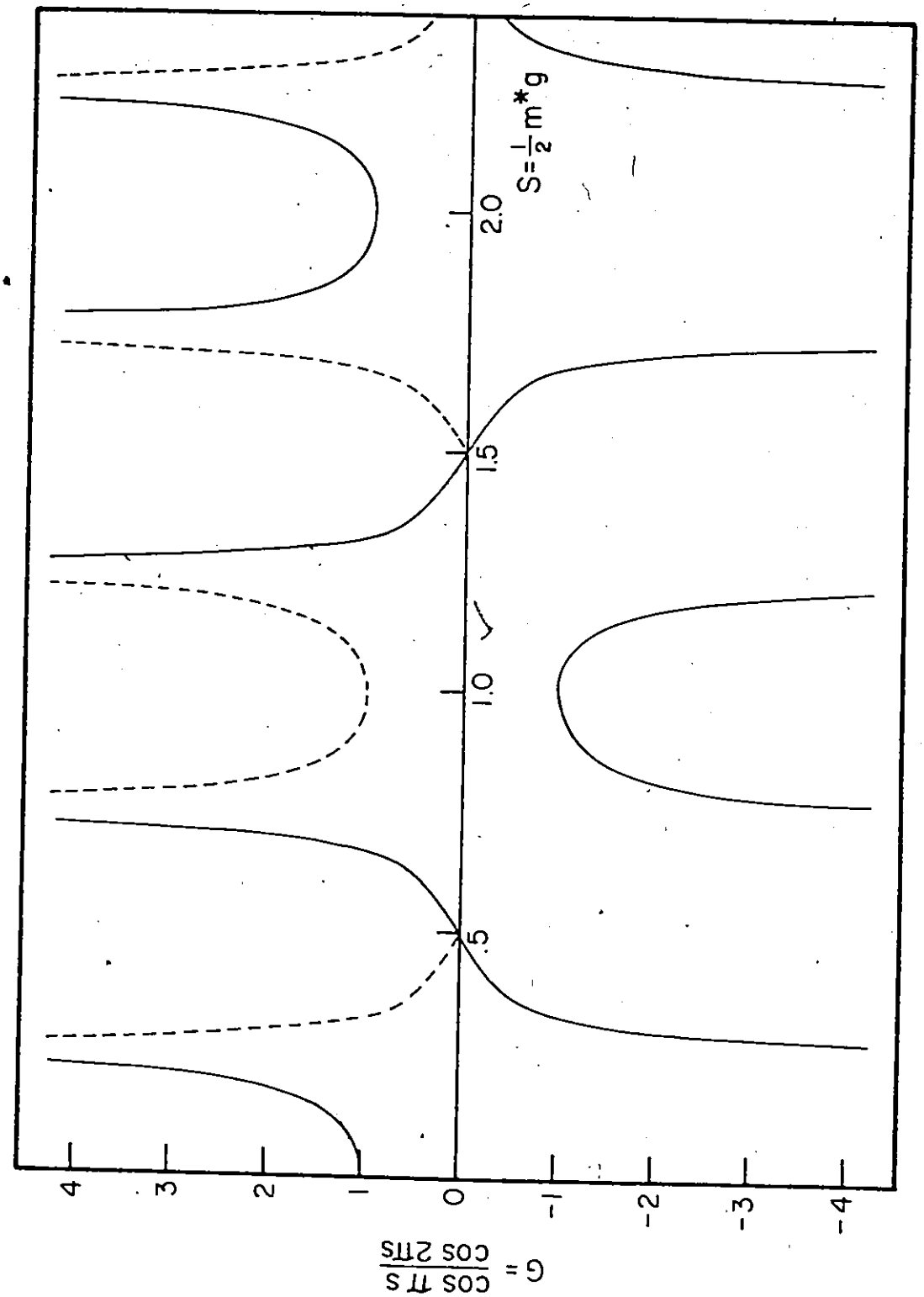

Fig. 3 The harmonic amplitude ratio, G, as a function of $S = \frac{1}{2} m^* g$

the behaviour of G as a function of S. In the absence of absolute phase measurements for both the fundamental and the second harmonic only the absolute value of G can be calculated. As shown in Figure 3 an ambiguity exists, as n±S will give the same harmonic amplitude ratio as S when n is any integer. This gives several possible g-values consistent with the measured amplitude ratio. Spin-zeros, orientations where the first harmonic amplitude is zero, are very useful in selecting possible g-values because S must be an odd half-integer and g can be narrowed down to two possible values in most cases. The ambiguity can also be reduced if $|G| < 1$.

Another method for measuring the g-factors is the direct observation of spin-splittings. In the torque method, at sufficiently high magnetic fields the spin-splittings can be directly observed and the g-factors could be calculated without a knowledge of the Dingle temperature. If the dHvA peaks are split by an amount δ in units of (1/H) and the corresponding peak separation in (1/H) of the fundamental dHvA frequency is 1/F, then

$$\frac{m^*}{m_s} = n \pm \delta F \qquad \text{[IV-8]}$$

where n is an integer, m_s is the spin-mass defined as $m_s/m_o = 2/g$ (Cohen and Blount 1960). One can write

$$g = \frac{2}{m^*} (n \pm \delta F) \; . \qquad \text{[IV-9]}$$

Here again the same ambiguity exists as any integral value for n will be consistent with the experimental data.

The advantage of using all three different methods, the torque-harmonic ratio, the field modulatio. harmonic ratio, and the direct observation of spin-splittings is that the non-linear effects discussed below affect the three methods differently and therefore agreement among them is a strong indication of the reliability of the conclusions drawn from the experiments.

4. NON-LINEAR EFFECTS

In measurements of cyclotron masses, Dingle temperatures and g-factors using the harmonic ratio method, the temperature and field dependence of the dHvA amplitude is investigated. Therefore, care must be taken to exclude or take account of any effects that change the dHvA amplitudes from that given by the Lifshitz-Kosevich theory. These effects include magnetic breakdown, magnetic interaction, and non-linear effects introduced by the experimental conditions and sample imperfections.

4.1 Magnetic Breakdown

The phenomenon of magnetic breakdown drastically changes the amplitudes of the dHvA oscillations. This effect does not happen in semimetals and will not be discussed here. For a review see Stark and Falicov (1967).

4.2 Magnetic Interaction

The correct magnetizing field in the Lifshitz-Kosevich equation [11.6] is not the applied field H but the total induction field B. The replacement of H by B has a negligible effect on the slowly varying coefficients of the amplitudes A_r, but the phase is significantly modified.

$$M = \sum_r A_r \sin[2\pi r(\frac{F}{H+4\pi M} - \gamma) \mp \frac{1}{4} \pi] \qquad [IV-10]$$

The resulting modification of the amplitude becomes appreciable as kA_1 approaches unity, where $k = \frac{8\pi^2 F}{H^2}$ or in other words when the amplitude of the oscillations is comparable to the field spacing $\frac{H^2}{F}$ of the oscillations. Phillips and Gold (1969) have solved [IV-10] for the case $kA_1 < 1$ by a scheme of successive approximations. The result for terms involving only first and second harmonics is

$$M = A_1 \sin\theta + A_2 \sin(2\theta \mp \frac{1}{4} \pi) - \frac{1}{2} kA_1^2 \sin 2\theta \qquad [IV-11]$$

where $\theta = 2\pi(\frac{F}{H} - \gamma) \mp \pi$. In this limit the fundamental amplitude is unchanged but the second harmonic is modified by a component of amplitude $f_2 = \frac{kA_1^2}{2A_2}$ times the ideal Lifshitz-Kosevich term and of phase differing by $\frac{1}{4} \pi$. Substituting for k, A, and M_2 results

$$f_2 = \frac{4\sqrt{2}\,\pi^2 \lambda T F^2}{H^{5/2}} \left|\frac{\partial^2 A}{\partial k_z^2}\right|_{ext}^{-1/2} \frac{\sinh(2\alpha m^* T/H)}{\sinh(\alpha m^* T/H)} G \qquad [IV-12]$$

f_2 is independent of T_D, and for the limit $\alpha m^* T/H > 1$ varies as $T/H^{5/2}$ so that at very low temperatures and high magnetic

fields this correction term is greatly reduced in this limit ($kA_1 < 1$). Equation [IV-12] also shows that f_2 is proportional to F^2, i.e. magnetic interaction effects can be neglected for low dHvA frequencies. In fact f_2 for the case of Sb is of the order of 10^{-3} at 1.3 K and at 2 T. Whereas for potassium $f_2 \sim .5$ at the same temperature and field values (Randles 1972).

For the limit $kA_1 \geq 1$, the oscillations become markedly distorted from a sine curve. The amplitude of the fundamental is still unchanged but the second harmonic amplitude is now given by $\frac{1}{2} kA_1^2$ and temperature dependences of dHvA amplitudes are now determined through $\frac{T^r}{\sinh(ram*T/H)}$ rather than $\frac{T}{\sinh(ram*T/H)}$ as in the Lifshitz-Kosevich theory.

Under certain circumstances, namely for a relatively high and isolated dHvA frequency the magnetic interaction effect can be a help rather than a hindrance and provides an independent g-factor measurement (Windmiller 1973). This is because the second harmonic of LK and MI amplitude terms differ in phase by $\frac{\pi}{4}$ and hence f_2 can be measured and [IV-12] solved for G without a knowledge of the Dingle temperature. However, for samples not in the form of long cylindrical rods, the R.H.S. of [IV-12] should be multiplied by (1-N), where N is the demagnetization factor.

4.3 Magnetic Field Inhomogeneity

The standard theory for the dHvA effect assumes a magnetic field which is homogeneous over the sample. Linear inhomogeneity makes the dHvA phase $2\pi\frac{F}{H}$ vary over the sample and thus cause the reduction of the dHvA amplitude. Hornfeldt et al. (1973) have shown that for cylindrical samples the dHvA amplitude in the presence of an inhomogeneity in the magnetic field that produces a linear field gradient ΔH over the sample length 2L is given by:

$$M = A\, I_1 \sin 2\pi \frac{F}{H} . \qquad \text{[IV-13]}$$

The amplitude reduction factor I_1 is given by

$$I_1 = 2\,\frac{\sin\pi v}{\pi v}\,\frac{J_1(\pi uR/L)}{\pi uR/L} \qquad \text{[IV-14]}$$

where $v = F\frac{\Delta H}{H^2}$, and $u = \left(\frac{\partial F}{\partial \theta}\right)_{max}\frac{\Delta H}{H^2}$, R is the radius of the sample. For Sb and the present experimental conditions, L and R are of order .1 cm, ΔH as determined from NMR calibration of the superconducting magnet is less than 1 Gauss. Thus $v \sim 10^{-4}$ and $u < v$, so that $I_1 = 1.000$.

4.4 Non-linearity in the Field Modulation Technique

There are two major causes of non-linear effects that change the harmonic amplitude ratio in the field modulation technique and these should be overcome or accounted for in the calculations.

One of the effects occurs when there is incomplete sample penetration of the modulating field. If the skin depth δ is smaller than the sample dimension then the Bessel function $J_2(2\pi rFh/H^2)$ in the expression for the measured dHvA amplitudes will not have the same value of h in all parts of the sample and the measured dHvA amplitudes will have an extra field dependence which can introduce errors in the results. To overcome this problem a sufficiently low modulation frequency is used to insure complete sample penetration.

The magnetoresistance tensor components of Sb at low temperatures are measured by Bresler and Red'ko (1972). The worst case or the smallest value for the skin depth can be estimated from the smallest component of the magnetoresistance tensor. This has a value of 1.38×10^{-6} ohm-m at 1.5 K in a magnetic field of 10 kOe. The resulting lower limit for the skin depth is 2.6 cm for a modulation frequency of 517 Hz. The samples used in dHvA modulation technique were roughly in cubic geometry with a side of about .2 cm.

The other effect is the so-called FM-AM effect described by Alles and Lowndes (1973). This effect is present whenever there is a high dHvA frequency f_1 and a low dHvA frequency f_2. The FM-AM effect is a periodic amplitude modulation (AM) of the high frequency oscillation (FM) with the period of the low frequency oscillation. This results in a swing Δa in the argument a of the Bessel function $J_n(a)$ given by $\frac{\Delta a}{a} = 4\pi \frac{\partial M_2}{\partial H}$ of the low frequency oscillation. In Sb, the dHvA frequencies

are all relatively low so that $4\pi \frac{\partial M}{\partial H} << 1$. Moreover in the present investigation almost all of the data are carried out for the dominant low frequency portions of the dHvA frequency branches.

4.5 The Torque-Interaction Effect

In the torque method non-linearities are introduced by the torque interaction effect (Vanderkooy and Datars 1968). It occurs when the torque on the sample causes an appreciable twisting of the sample. If the elastic compliance of the sample about the direction of suspension is $\eta = \frac{\partial \theta}{\partial \tau}$, the torque τ is given by

$$\tau = - \frac{\partial \phi}{\partial \theta} = A \sin(2\pi \frac{F}{H}) . \qquad [IV-15]$$

For a torque τ, the angle θ changes from its equilibrium position by an amount $\Delta\theta = \eta\tau$ which changes the initial frequency F_o to $F(\theta + \Delta\theta)$. Equation [IV-15] then becomes

$$\tau = A \sin(\frac{2\pi F_o}{H} + \frac{2\pi}{H} \frac{\partial F}{\partial \theta} \eta\tau) . \qquad [IV-16]$$

This is similar to the case of magnetic interaction and can cause non-sinusoidal solutions and influences the harmonic amplitude ratios for $\left|\frac{2\pi}{H} \frac{\partial F}{\partial \theta} \eta\tau\right| \geq 1$.

Vanderkooy and Datars (1968) give an expression for the ratio Γ of the torque interaction to the magnetic interaction contributions to the dHvA amplitude,

$$\Gamma = \frac{\eta V H^2}{4\pi} \xi \qquad [IV-17]$$

where V is the sample volume, and the dimensionless parameter ξ depends on the geometry of the Fermi surface. An estimate of Γ is 10 at H = 20 kOe for the estimated values $\eta \sim 10^{-5}$ Rad/dyne-cm, $\xi_{max} \sim 1$ (for ellipsoids with b/a>2), $V \sim .05$ cm^3. This value for Γ suggests that in the torque method the torque interaction is much more important than the magnetic interaction contribution. Nevertheless, as the magnetic interaction contribution was estimated previously to be less than 10^{-3}, the torque interaction is also negligible under the present experimental conditions for Sb. This would not be true if large samples had been used.

4.6 Crystal Imperfections

Finally there are non-linear effects that depend on crystal imperfections. These include lattice strain and mosaic structure. In general, these effects are rather difficult to treat quantitatively, but as these effects are all field dependent they produce non-linearities in the Dingle plots. Thus all samples exhibiting non-linear behaviour in the Dingle plots were discarded. (Crystal imperfections were sometimes detected, during crystal orientation, by the X-ray diffraction Laue photographs from an examination of the structure of the Laue spots and these samples were also discarded).

5. INFINITE FIELD PHASE

The harmonic amplitude ratios or spin-splittings can only provide the absolute value of G. However from absolute phase measurements on the fundamental and second harmonic oscillations one can obtain the infinite field phase which can have two possible values depending whether the spin-splitting term, $\cos(\pi r S)$ is positive or negative (Coleridge and Templeton, 1972). This procedure reduces drastically the number of possible g-factors obtained from harmonic amplitude ratio measurements. The total phase, ϕ_T, at a positive peak of the dHvA fundamental oscillation is given by

$$\phi_T = \frac{F}{H} + \phi_H = \frac{F}{H} + \frac{1}{4} - \gamma \mp \frac{1}{8} \mp \frac{1}{4} \qquad \text{[IV-18]}$$

where ϕ_H is the local phase, and the last $\mp$ sign corresponds to the spin-splitting term being positive or negative respectively. In antimony the extremal areas are of maximum area, and taking $\gamma = \frac{1}{2}$ the total phase becomes

$$\phi_T = \frac{F}{H} - \frac{3}{8} \mp \frac{1}{4} . \qquad \text{[IV-19]}$$

The infinite field phase, ϕ_o, (when $\frac{1}{H} = 0$) can have the values $-\frac{1}{8}$ or $-\frac{5}{8}$ depending whether the spin-splitting term is positive or negative respectively. The local phases $\frac{F}{H} - N$, where N is Landau level number, at the positive peak are plotted against $\frac{1}{H}$. The intercept of a least squares fit at $\frac{1}{H} = 0$ then gives the infinite field phase ϕ_o.

CHAPTER V

EXPERIMENTAL RESULTS

The dHvA measurements were made in the trigonal-bisectrix and trigonal-binary planes. Figures 4-7 show the dHvA frequencies as a function of angle for the four alloy samples in the trigonal-bisectrix plane. The overall quality of the data decreased as the tellurium concentration increased, since alloying raised the Dingle temperature. The trigonal-bisectrix plane contains the minimum principal frequencies of the hole and electron branches. The hole frequencies decrease and the electron frequencies increase as Te atoms are added. The decrease is about 20% that of pure Sb values and the increase is about 25% with the addition of .110 at. % Te.

Figure 8 shows the cyclotron masses at the principal electron and hole minima frequencies in the trigonal-bisectrix plane vs. concentration of Te and Sn. The Sb(Sn) data were obtained previously by Dunsworth and Datars (1973). The hole mass decreases with increasing concentration of Te while the electron mass increases. Table 2 summarizes the data at the principal electron and hole minimum frequencies. The high values for T_D suggest that the Landau level broadening is the result of dislocations produced in the crystal while alloying and thermal cycling. T_D for the hole minimum of samples 1 and

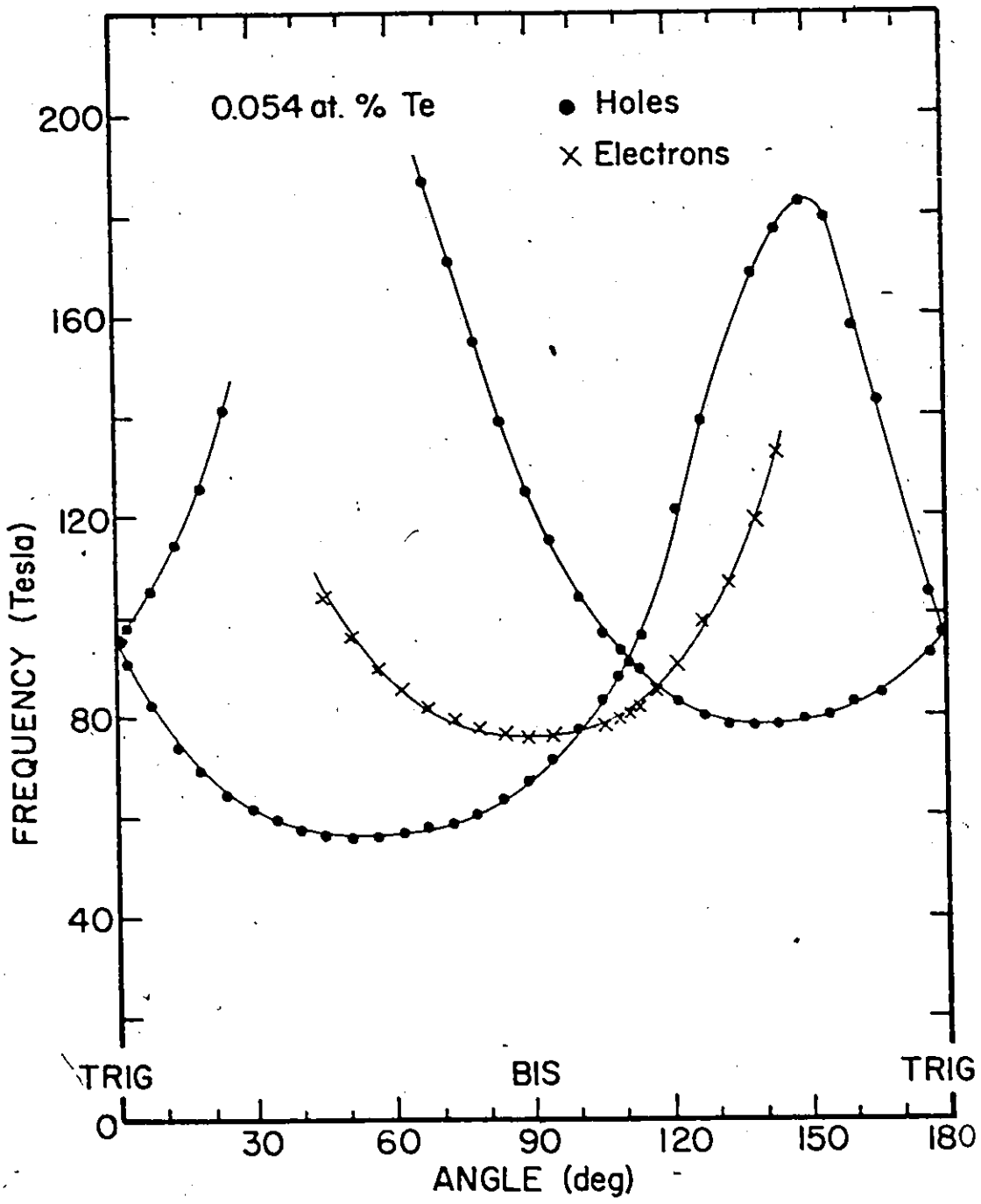

Fig. 4 dHvA frequencies for 0.054 at. % Sb(Te) alloy for field directions in the trigonal-bisectrix plane.

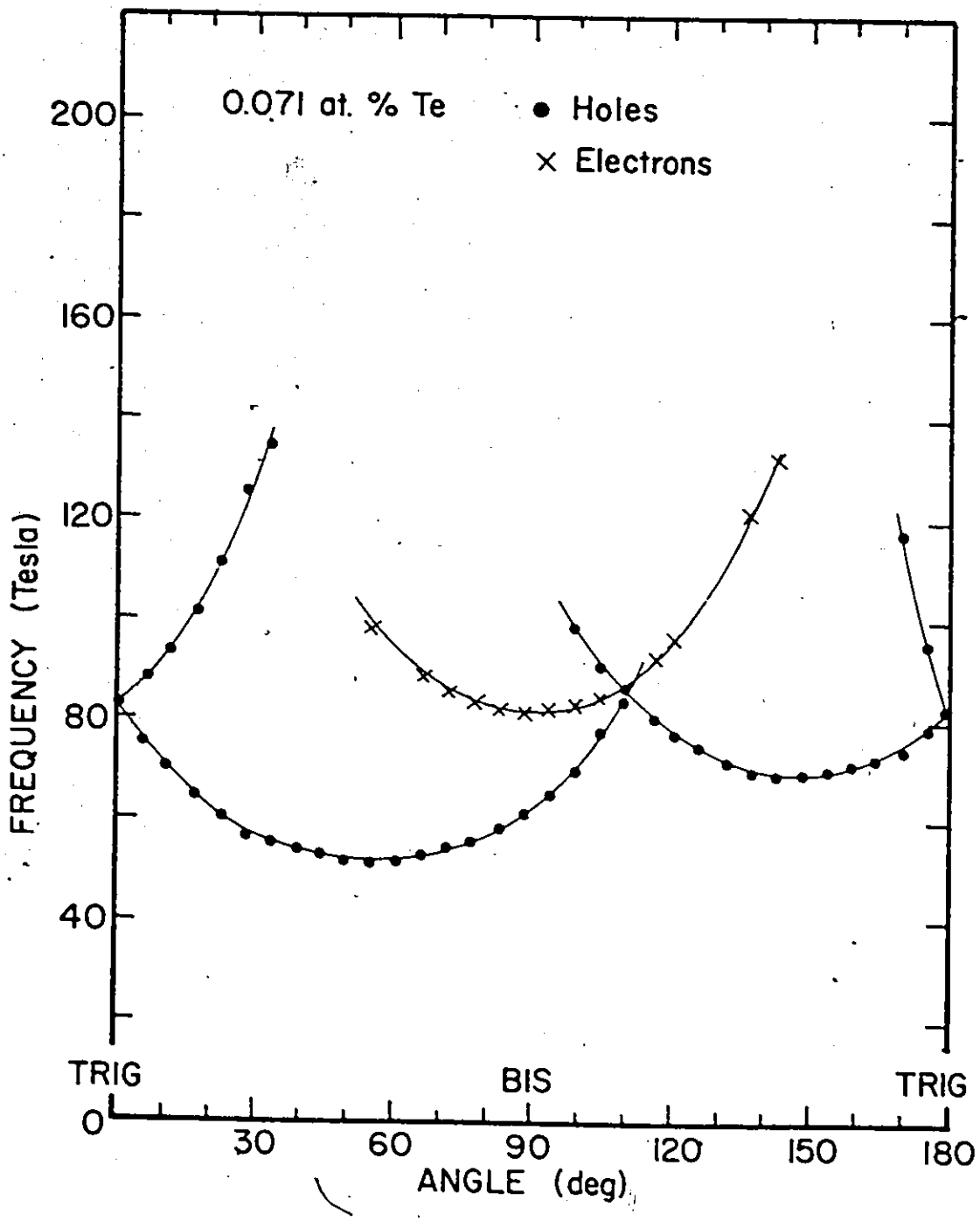

Fig. 5 dHvA frequencies for 0.071 at. % Sb(Te) alloy for field directions in the trigonal-bisectrix plane.

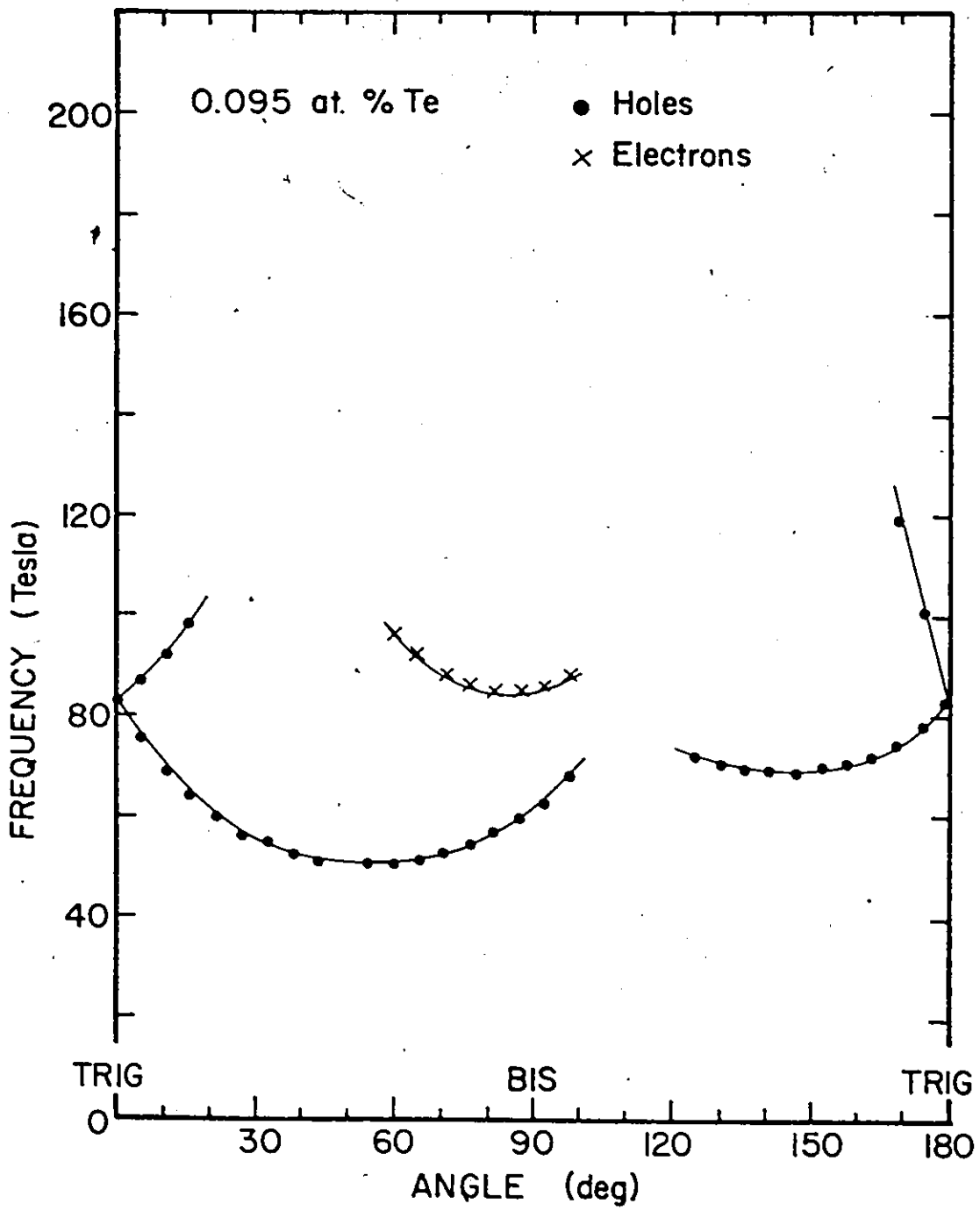

Fig. 6 dHvA frequencies for 0.095 at. % Sb(Te) alloy for field directions in the triconal-bisectrix plane.

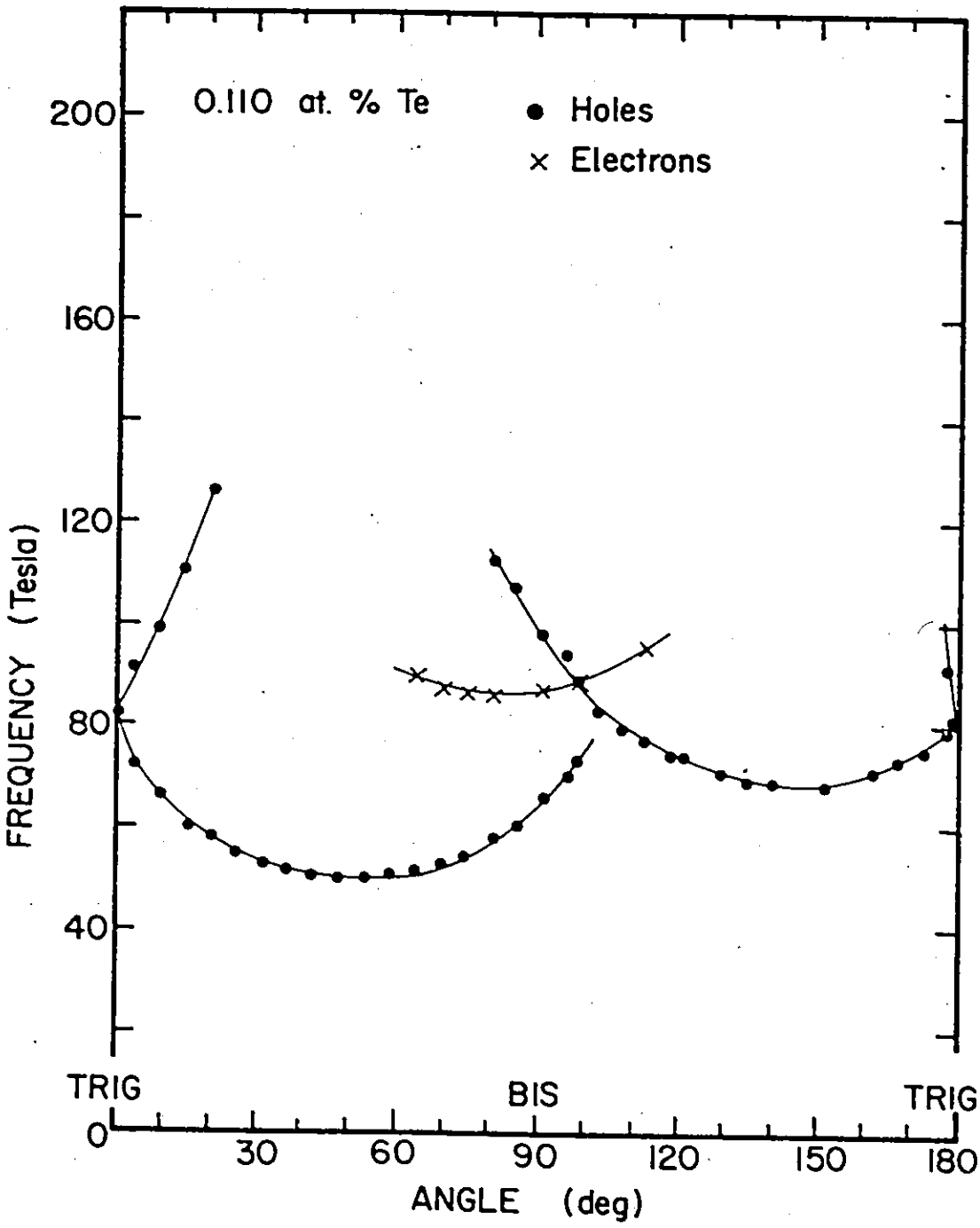

Fig. 7 dHvA frequencies for 0.110 at.% Sb(Te) alloy for field directions in the trigonal-bisectrix plane.

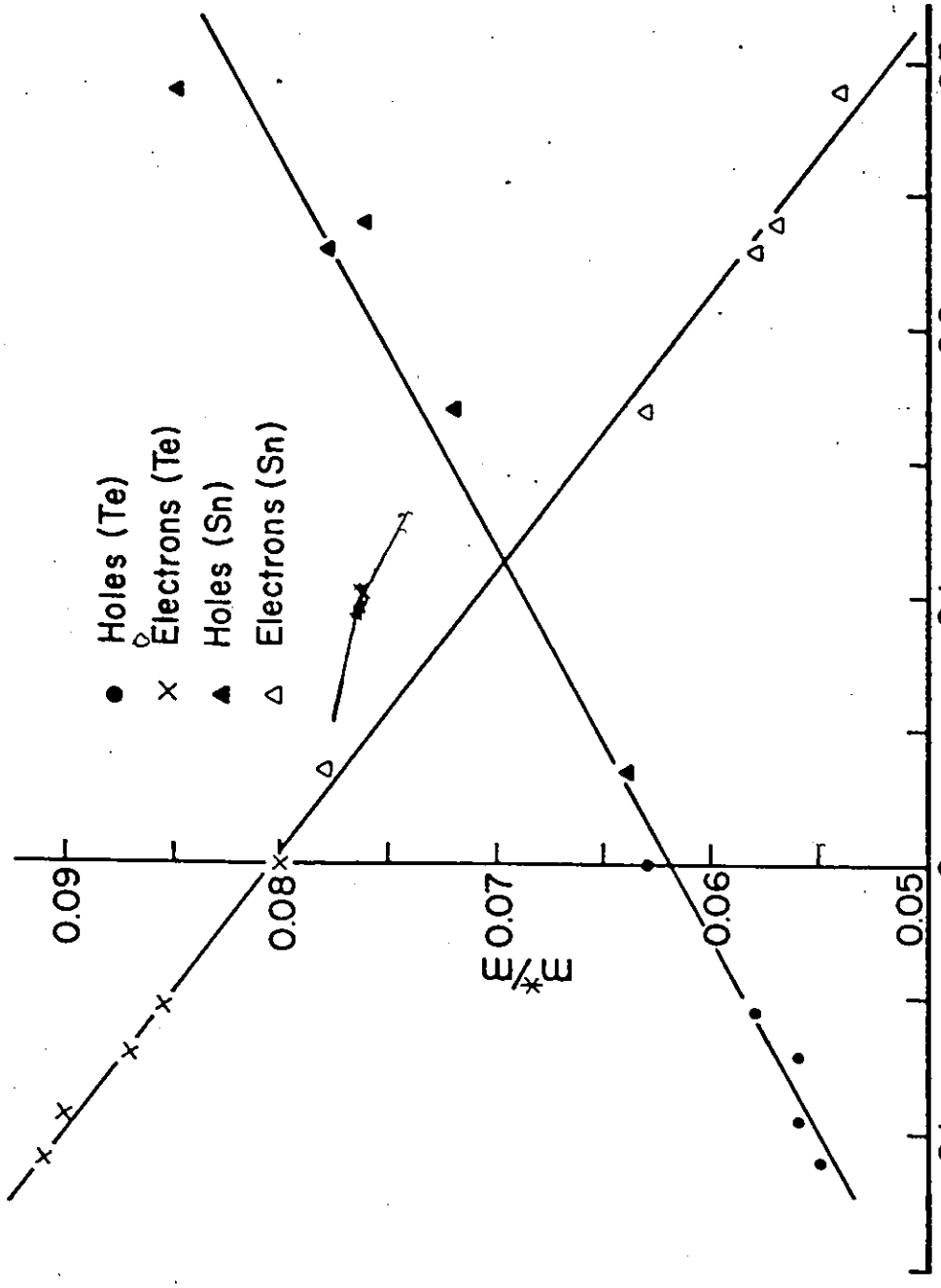

Fig. 8 Dependence of cyclotron mass on Te and Sn concentrations at electron and hole minima.

2 was investigated first, while, for sample 3, T_D at the electron minimum was determined first. During the orientation of sample 1 prior to the measurement of T_D at the electron minimum, a malfunction in the rotation mechanism caused some damage to the crystal. This explains the relatively high T_D for this sample. As the Dingle temperature depends on the history of the crystal as well as impurity scattering, conclusions about Dingle temperatures for different carriers could not be made.

Figure 9 shows the dHvA frequencies in the trigonal-bisectrix and the trigonal-binary planes for pure Sb obtained by the field modulation technique for g-factor measurements. Due to the high sensitivity of the technique it was possible for the first time to detect the high frequency electron branch in the vicinity of the bisectrix axis in the trigonal-bisectrix plane. The harmonic amplitude ratios were obtained for both the principal (P) and non-principal (NP) hole branches, while for the electrons only the principal branch was investigated. Using the torque magnetometer a smaller frequency range was studied: the harmonic amplitude ratios could not be determined at orientations where the torque vanishes near symmetry and frequency extrema directions. It should also be pointed out that the low frequency oscillations are dominant in the torque method and this prevented accurate measurements of harmonic amplitude ratios of the high frequency portions of the hole and electron branches.

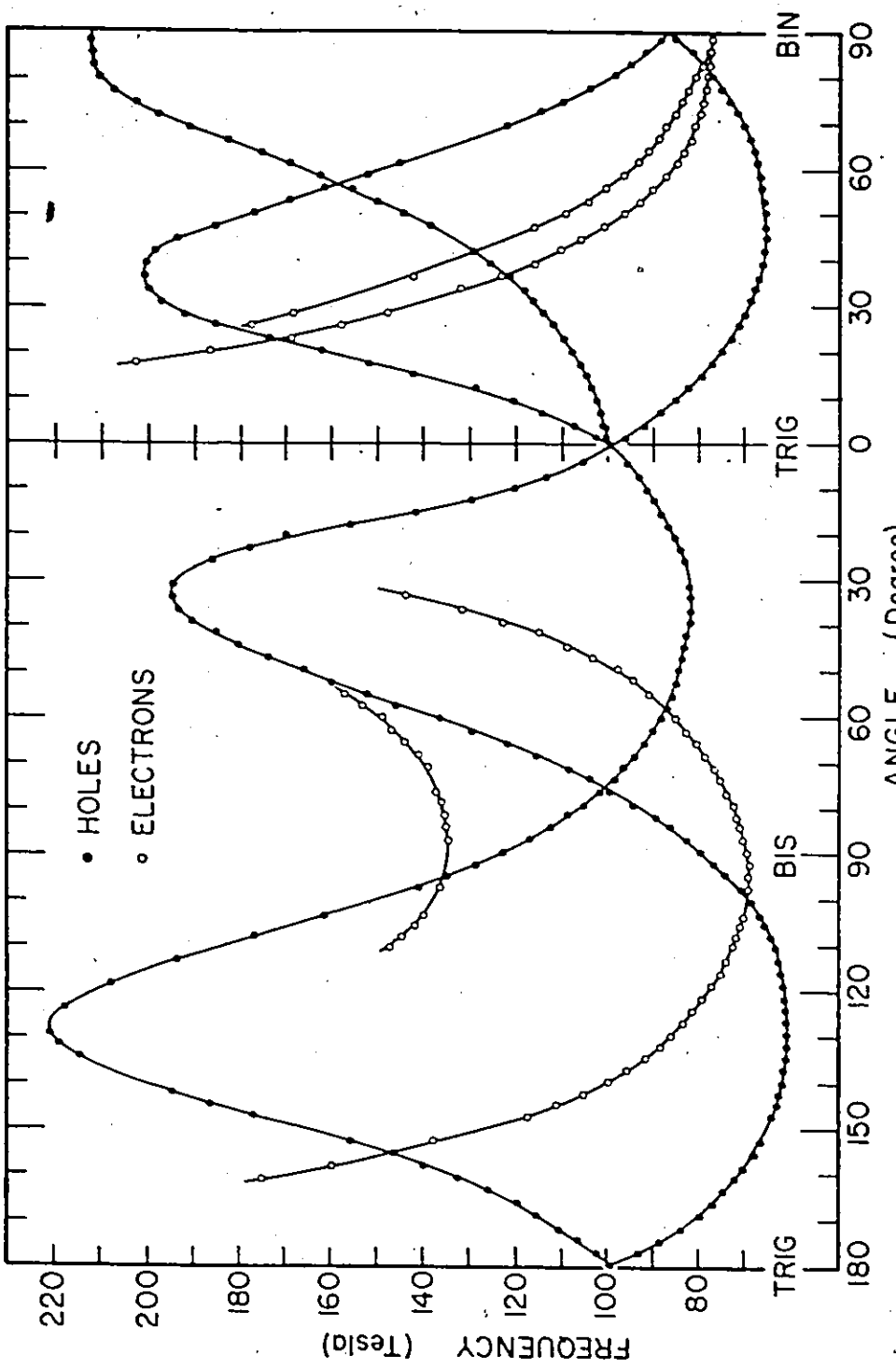

Fig. 9 dHvA frequencies for pure Sb for field directions in the trigonal-bisectrix and trigonal-binary planes.

Table 2. dHvA frequencies, cyclotron masses and Dingle Temperatures in Sb(Te) Alloys

Te concentration at. %	0.000	0.054	0.071	0.095	0.110
Minimum electron freq. (Tesla) in trig-bis plane	68.0	75.8	81.5	85.0	86.0
Cyclotron mass (m_o) electron minimum	0.080	0.085	0.087	0.090	0.091
Dingle Temp. (K) electron minimum	2.9	7.7	5.7	6.1	-
Minimum hole freq. (Tesla) in trig-bis plane	61.5	56.1	51.8	50.6	49.9
Cyclotron mass (m_o) hole minimum	0.063	0.058	0.056	0.056	0.055
Dingle Temp. (K) hole minimum	2.5	5.4	5.2	6.4	-

Typical Fourier transforms are shown in Figs. 10 and 11 for field directions at 10° and 26° from the trigonal axis in the trigonal-bisectrix plane respectively. The amplitude of the second harmonic, 2H, with respect to the fundamental amplitude H, in Fig. 11 is three times that in Fig. 10. This is caused in part by a change in the g-factor.

Figures 12 and 13 show typical Dingle plots for the field modulation and the torque method respectively. The plots are straight lines ruling out any phase smearing processes which produce a field-dependent T_D.

In the torque method, at sufficiently high magnetic fields, greater than 40 kOe, the spin-splittings were directly observed for several orientations and the g-factors were independently calculated. Figure 14 shows such a spin-splitting recorder tracing for holes at 148° from the trigonal axis in the trigonal bisectrix plane.

To obtain a value for G ($G = \cos(\pi S)/\cos(2\pi S)$), for each position the dHvA amplitudes for the fundamental and second harmonic frequency prior to Fourier analyses were multiplied by their appropriate field-dependent correction terms. It was found advantageous not to include the Bessel function term in the field modulation method by choosing the data between appropriate but different field limits for the fundamental and second harmonic in such a way that both data cover the same Bessel function values throughout. This was necessary to avoid multiplying the experi-

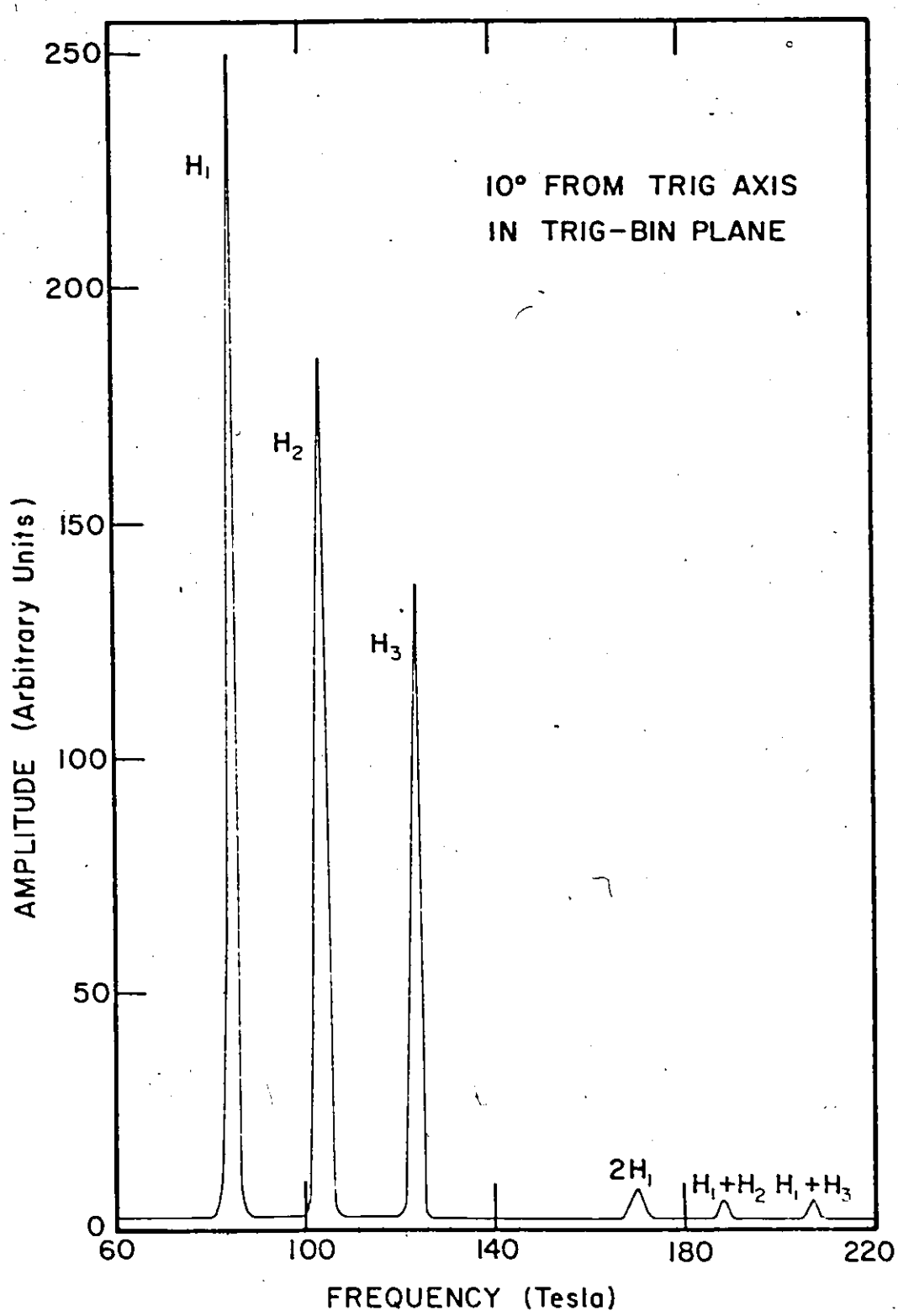

Fig. 10 Fourier transform for field direction at 10° from trigonal axis in the trigonal-bisectrix plane.

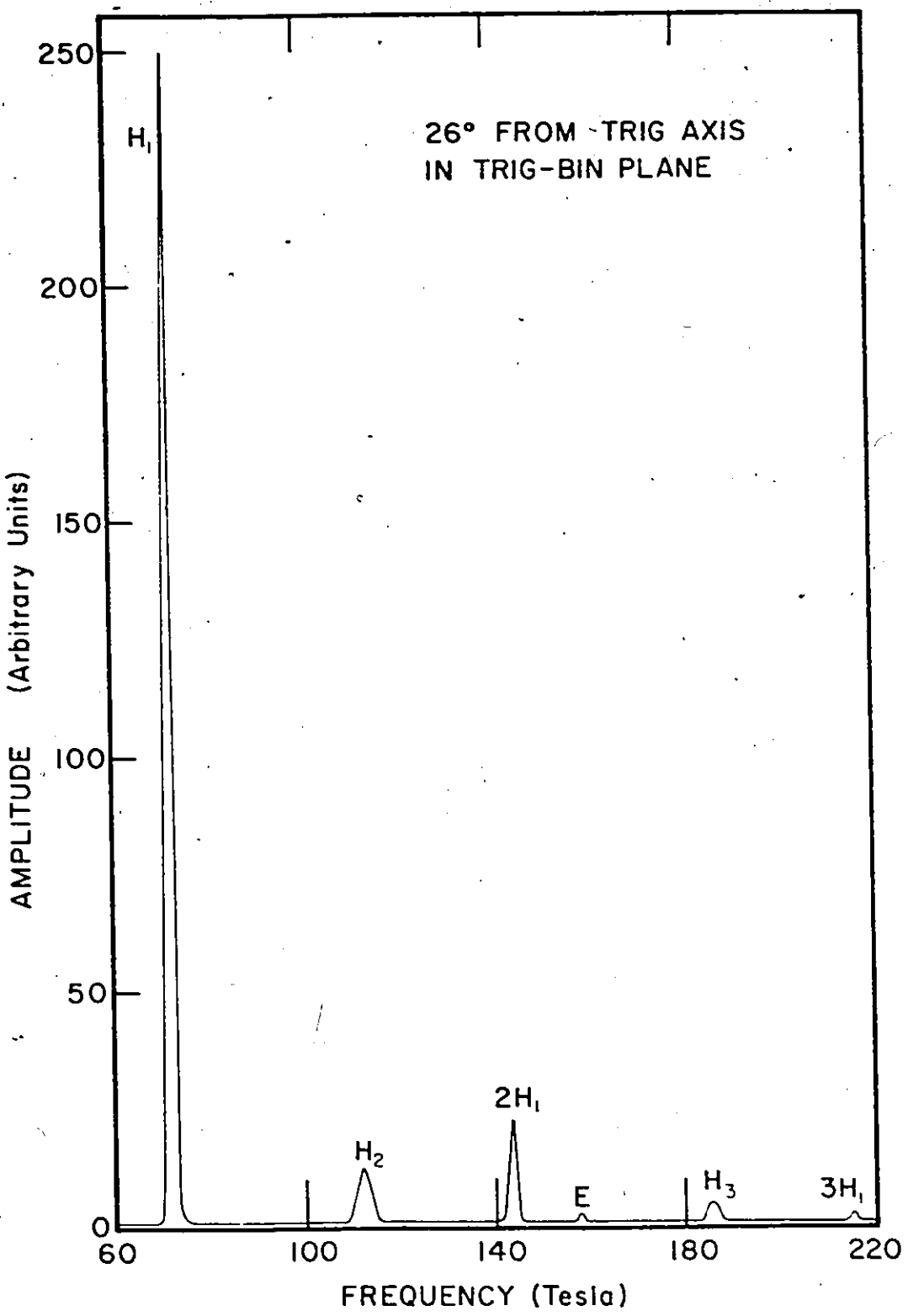

Fig. 11 Fourier transform for field directions at 26° from trigonal axis in the trigonal-bisectrix plane.

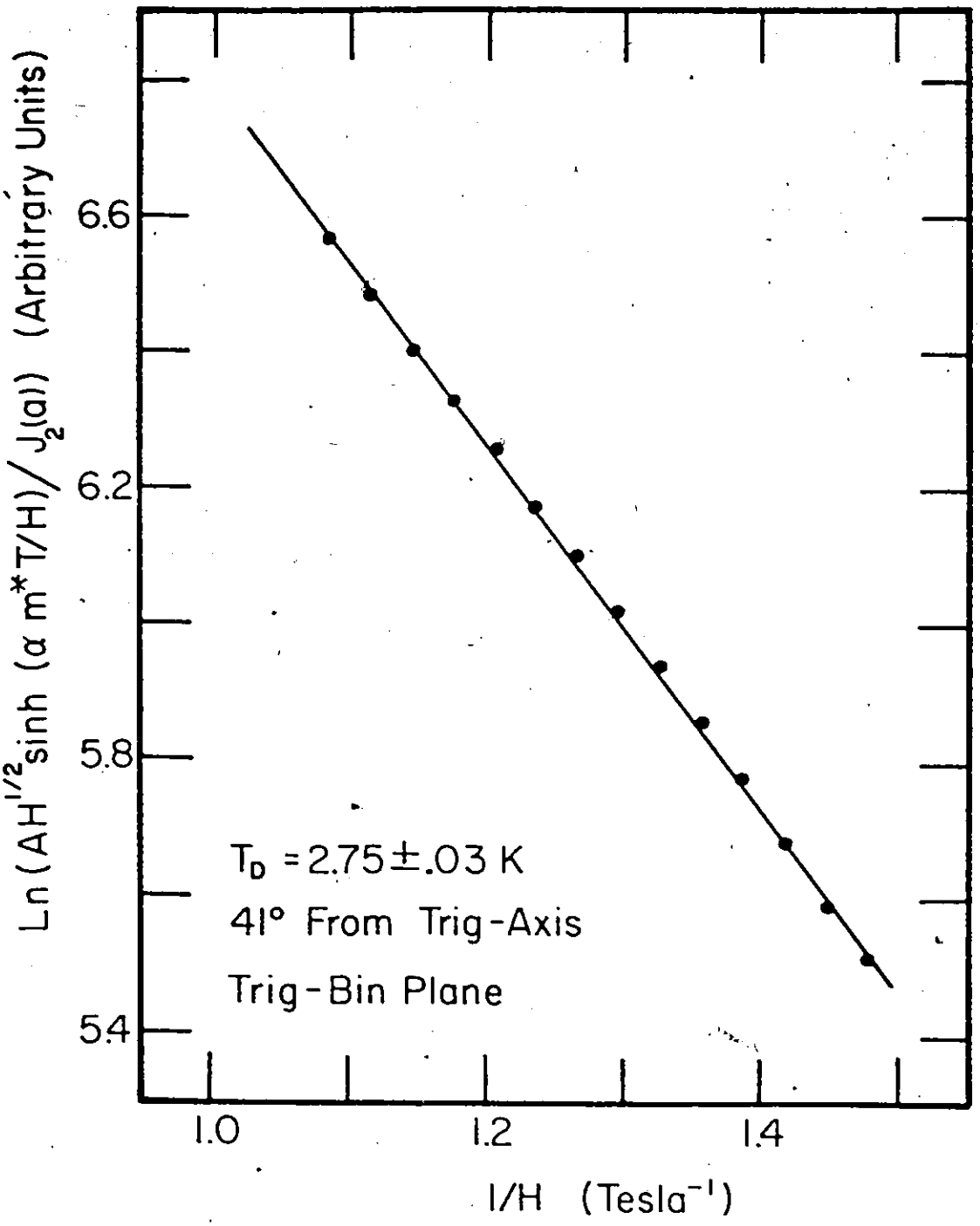

Fig. 12 Hole Dingle plot (field modulation method) for field direction at 41° from the trigonal axis in the trigonal-binary plane.

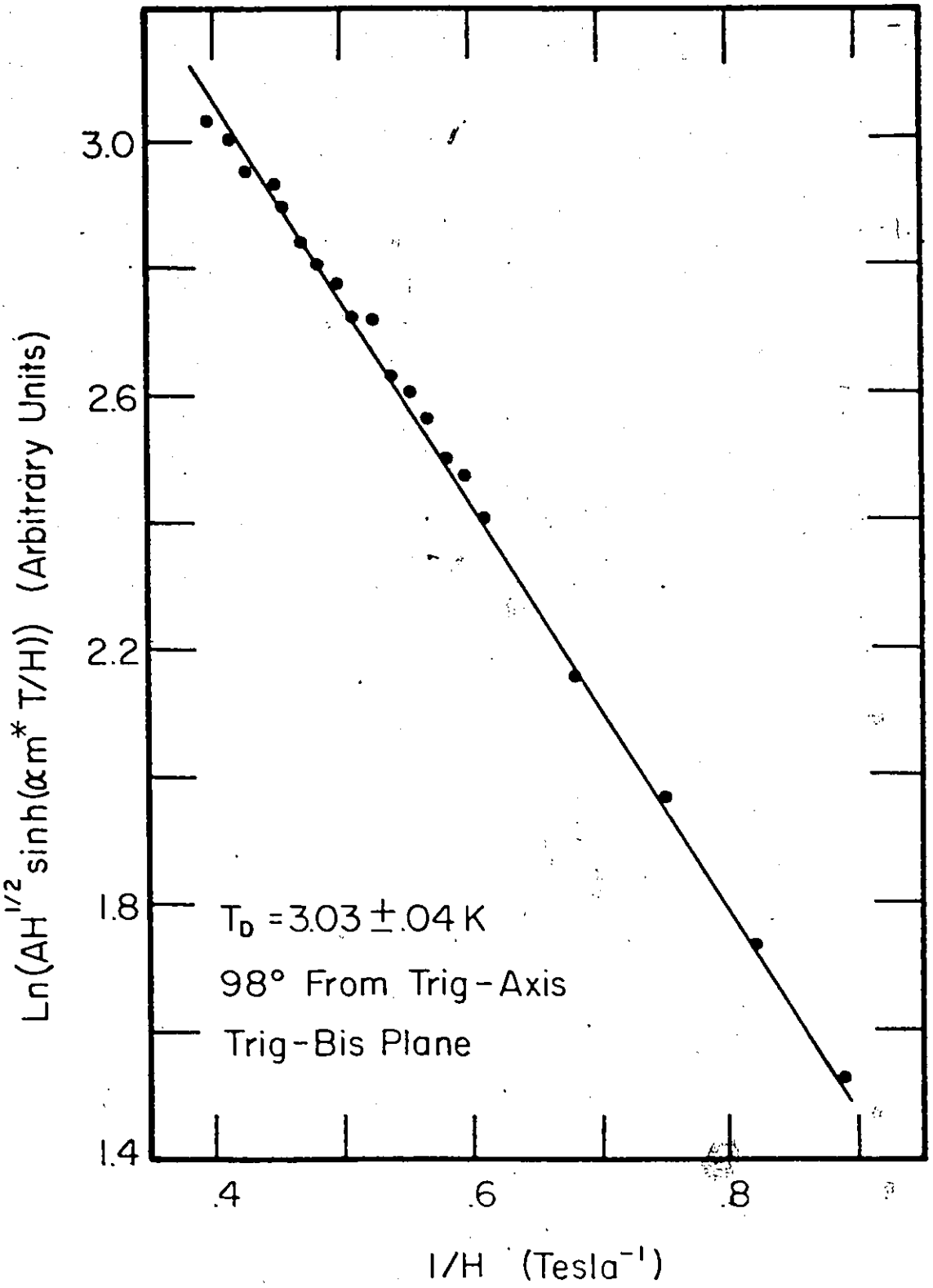

Fig. 13 Dole Dingle plot (torque method) for field direction at 98° from the trigonal axis in the trigonal-bisectrix plane.

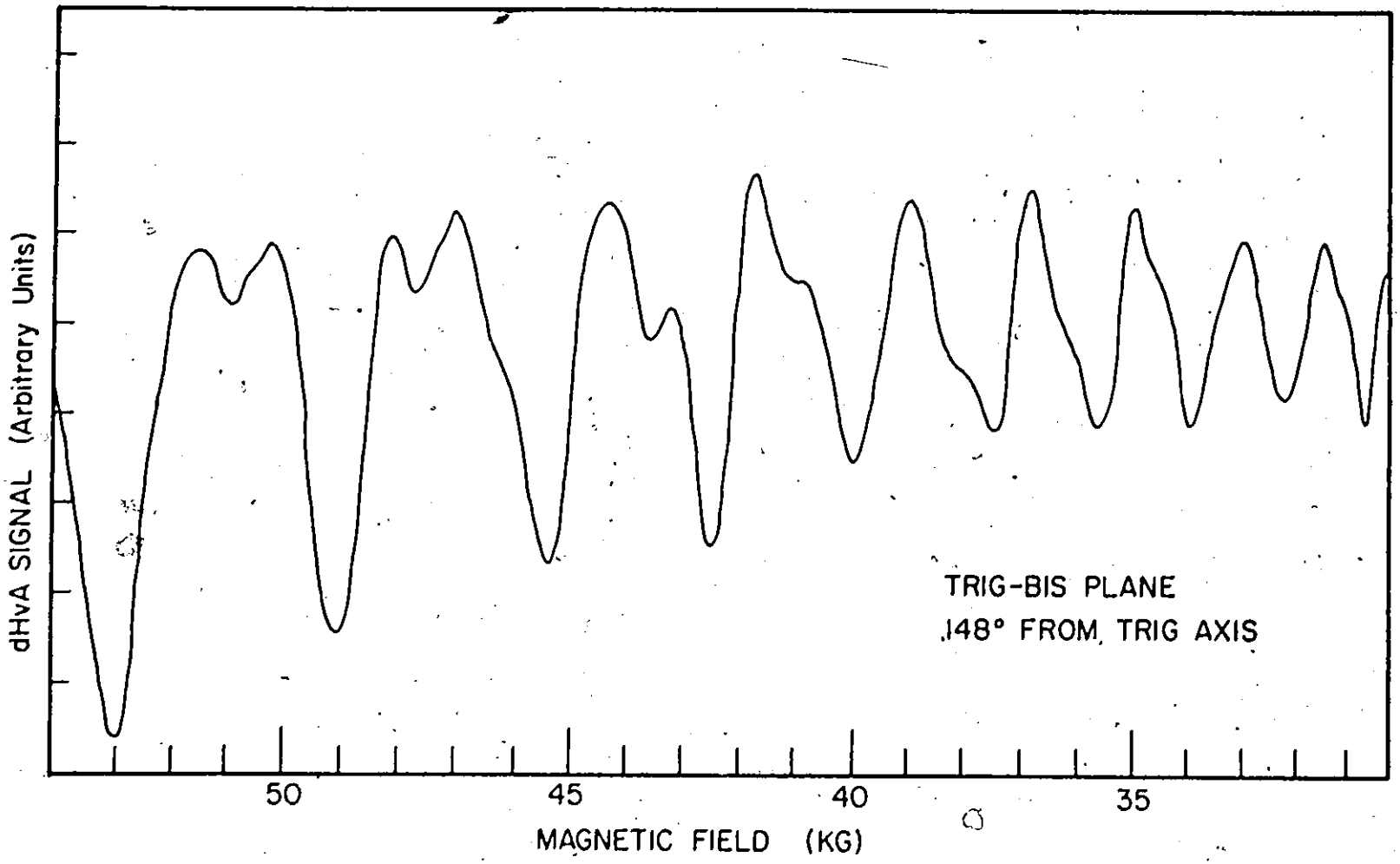

Fig. 14 Hole spin-splittings in the dHvA torque oscillations at 148° from the trigonal axis in the trigonal-bisectrix plane.

mental amplitudes by large factors near Bessel zeros and at the same time taking advantage of a maximum number of oscillations.

Reliable and accurate absolute phase measurements are generally done when there exists a single or well isolated dHvA frequency. The torque magnetometer provided an ideal technique in measuring infinite field phases for the electron frequency branch in the trigonal-bisectrix plane at a field direction where the dominant dHvA hole frequency passes through its minimum, i.e. $\frac{\partial F_h}{\partial \vartheta} = 0$ in equation [IV -5] and the hole oscillations disappear. At this position the infinite field phase for electrons, ϕ_o, as shown in Fig. 15, was found to be -.56±.05 indicating that the spin-splitting term for electrons is negative at this orientation.

Absolute phase measurements for the holes, on the other hand, were done using the modulation technique at field directions where the hole frequencies are dominant and no other dHvA oscillations virtually exist. The total phase in the case of the modulation technique has an additional phase change of $\frac{1}{4}$ when detecting the dHvA signal at the second harmonic of the modulation frequency according to equation [IV-4]. However, in order to use expression [IV-19] for the total phase, the local phases were measured at the negative peaks of the dHvA oscillations. The measurements were done at three different field directions near the principal branch frequency minimum in the trigonal-bisectrix plane for the principal hole branch. The results, an example is shown in Fig. 16, give ϕ_o = -.58±.05,

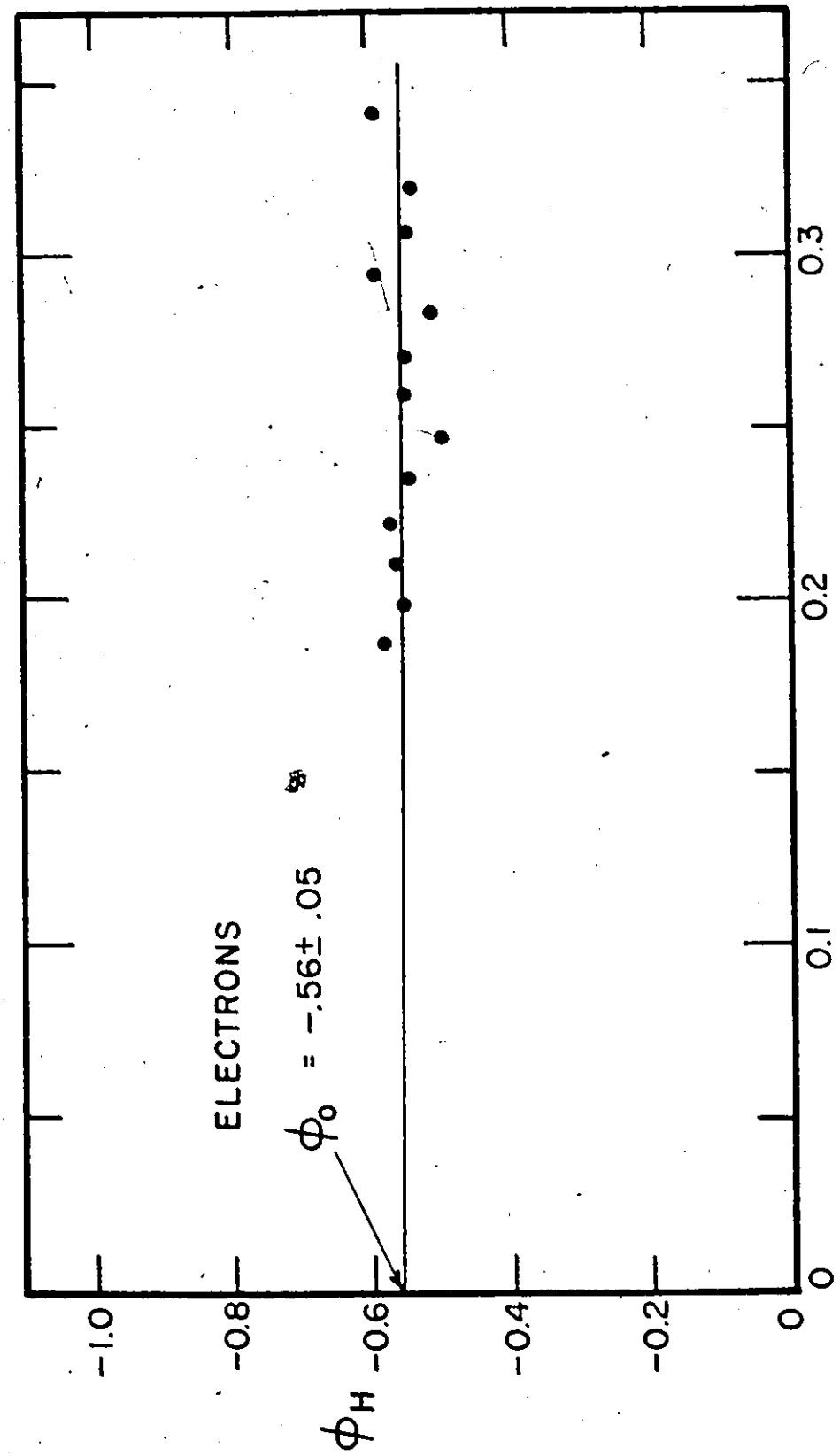

Fig. 15 ϕ_H, the dHvA local phase, versus 1/H for electrons at the hole frequency minimum in the trigonal-bisectrix plane.

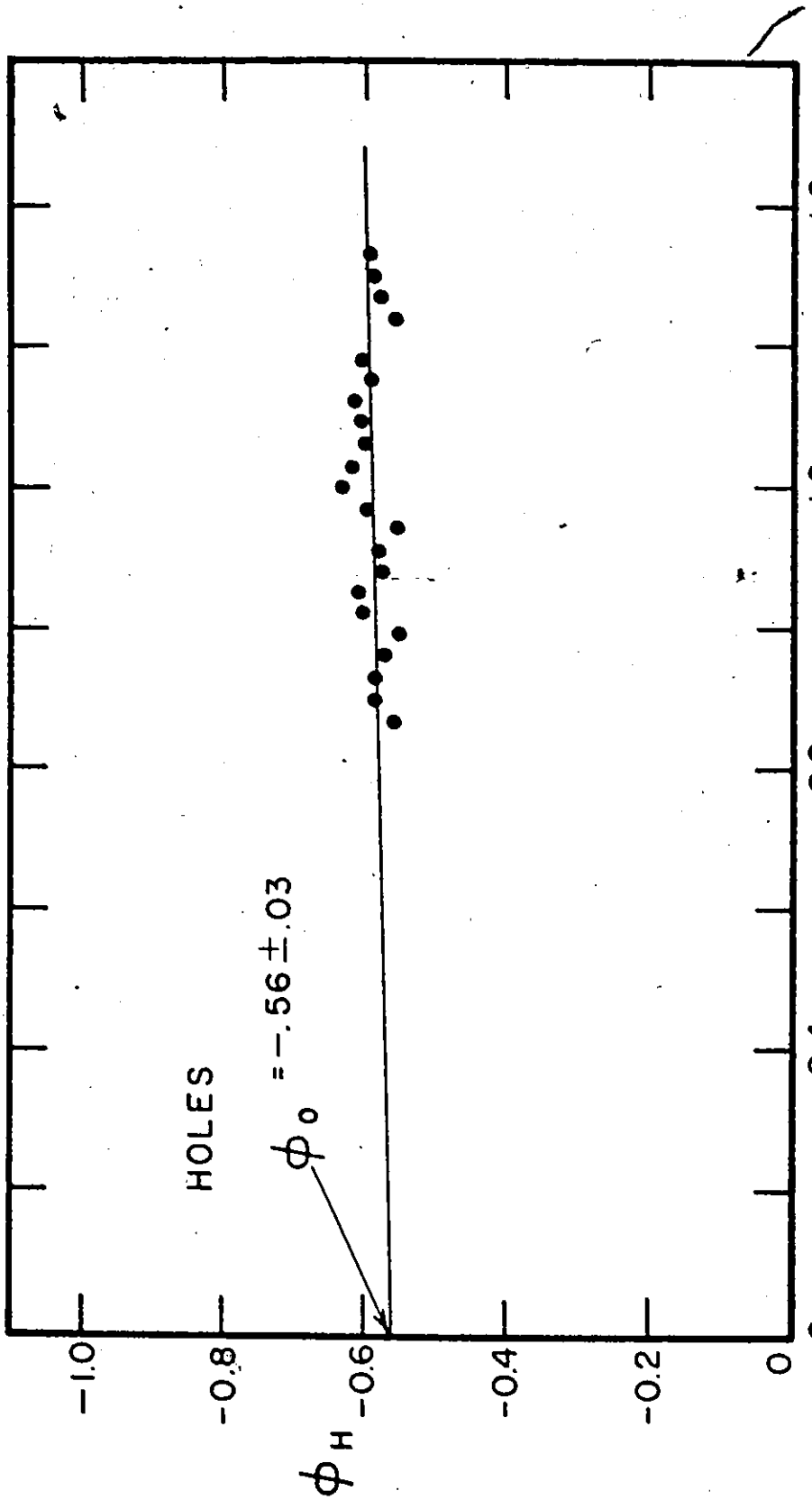

Fig. 16 ϕ_H, the dHvA local phase, versus 1/H for holes near the frequency minimum in the trigonal-bisectrix plane.

which shows that the spin-splitting term of holes is also negative. These results, combined with the fact that most of the measured harmonic amplitude ratios A_1/A_2 (including, of course, those at the spin zeros) are less than unity, indicate that the possible g-factors for both electrons and holes should lie on the two solid branches of Fig. 3 that intersect the S ($= \frac{1}{2}$ gm*) axis. It is evident that in the case of antimony absolute phase measurements on the fundamental dHvA oscillations alone were sufficient to resolve the g-factor ambiguities. Absolute phase measurements of the second harmonic would not have helped because the second harmonic would have yielded a negative spin-splitting term for all possible values of g. Finally, one has to consider a theoretical approach or make use of existing reliable spin resonance data to single out the correct g-factor from the branches having a negative spin-splitting term.

Figures 17 and 18 show the hole and electron g-factors respectively determined in the two planes by the three different techniques; torque harmonic ratio, field modulation harmonic ratio, and spin-splittings. Results are given for the first two possible g-factors. The g-factor results are also given in tabular form in Table 3 for selected crystallographic directions. For comparison the g-factors obtained by McCombe and Seidel (1967) from spin-splittings in the magnetothermal oscillations are also indicated in Table 3.

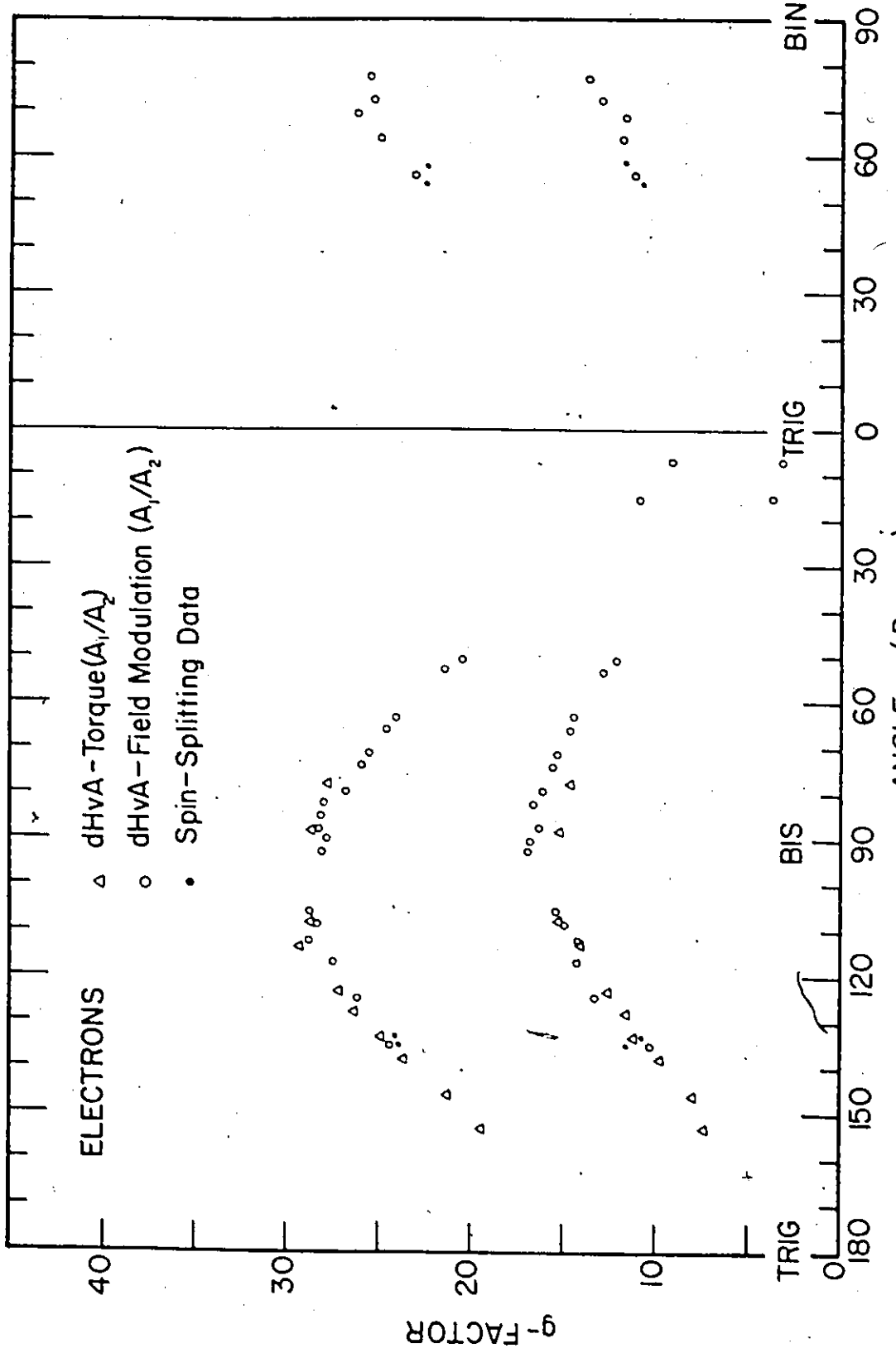

Fig. 17 Possible electron g-factors obtained by the torque (Δ), field-modulation (○) and the spin-splitting (•) in the trigonal-bisectrix and trigonal-binary planes.

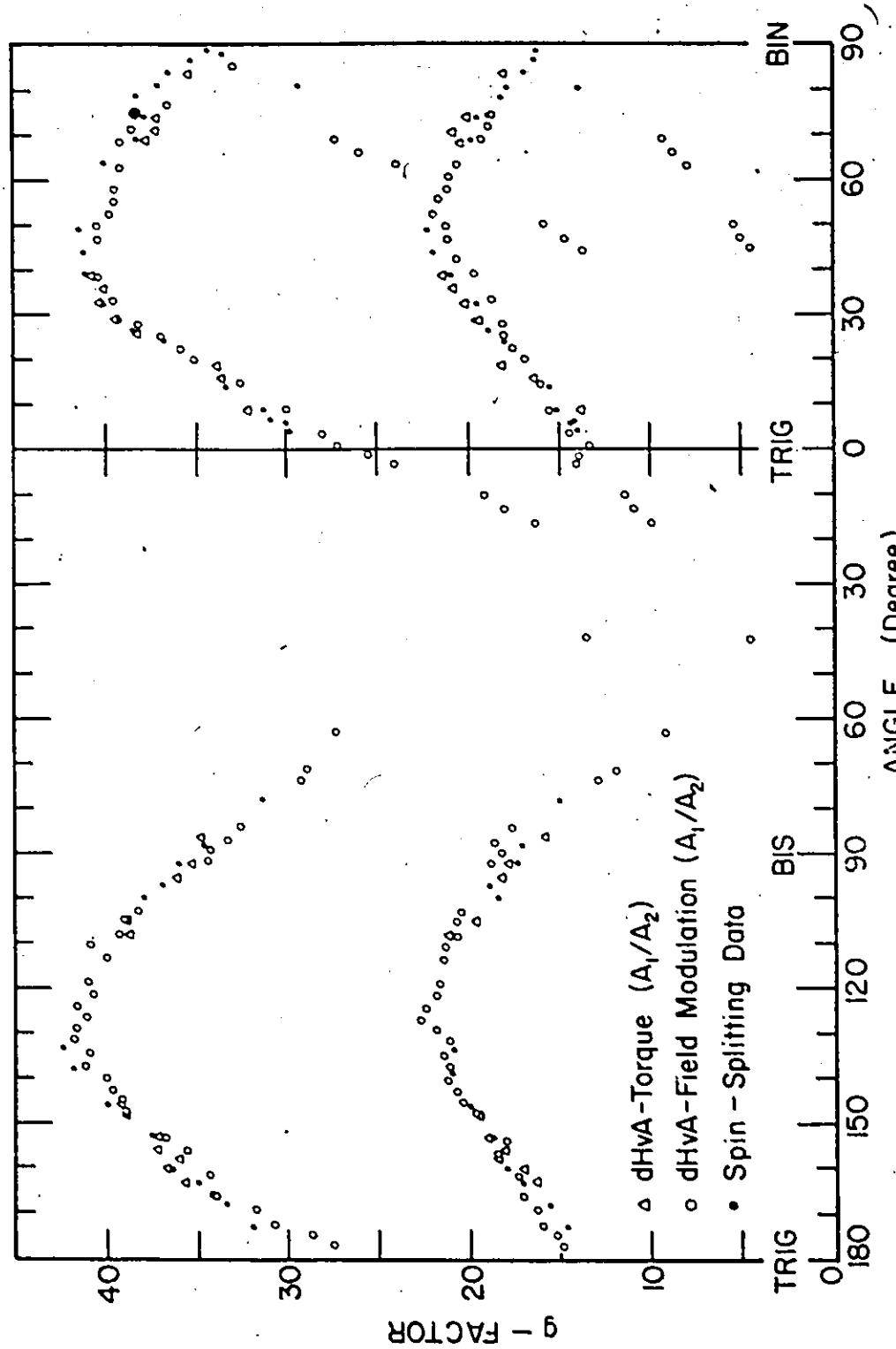

Fig. 18 Possible hole g-factors obtained by the torque (Δ), field-modulation (o) and the spin-splitting (•) in the trigonal-bisectrix and trigonal-binary planes.

Table 3 Antimony g-Factors

Trigonal-Bisectrix Plane					Trigonal-Binary Plane						
Position (deg.)	Electrons (P) $m_s>m^*$	Electrons (P) $m_s<m^*$	Holes (P) $m_s>m^*$	Holes (P) $m_s<m^*$	Position (deg.)	Electrons (P) $m_s>m^*$	Electrons (P) $m_s<m^*$	Holes (P) $m_s>m^*$	Holes (P) $m_s<m^*$	Holes (NP) $m_s>m^*$	Holes (NP) $m_s<m^*$
0(Trig.)	(3.5)[a]	(10)[a]	14.5	26.4	0(Trig.)	(3.5)[a]	(10)[a]	13.8	26.7	13.8	26.7
10	3.3	9.8	11.5	18.1	10	---	---	---	---	15.0	31.0
20	4.7	12.3	9.0	15.1	20	---	---	---	---	17.3	34.7
30	(7.2)[a]	(14)[a]	---	---	30	---	---	---	---	19.3	39.1
40	(9.5)[a]	(17.6)[a]	4.2	13.0	40	---	---	---	---	20.5	40.7
50	12.0	20.6	---	---	50	10.5	22.0	---	---	21.6	40.7
60	14.0	23.4	8.2	26.0	60	11.6	23.5	---	---	21.0	39.3
70	15.2	25.4	11.5	28.5	70	12.2	25.3	---	---	19.7	38.0
80	16.2	27.3	15.5	31.2	80	14.0	25.6	---	---	18.0	36.8
90(Bis.)	16.8	28.3	18.0	34.5	90(Bin.)	(15)[a]	(26)[a]	4.5	13.5	16.0	34.0
	18.2[b]	26.7[b]	22.7[b]	34.0[b]		15.8[b]	23.1[b]				
100	16.5	28.6	19.5	37.9	100	---	---	5.0	14.7	13.5	29.5
110	14.8	28.5	21.2	40.0	110	---	---	5.5	16.2	9.5	27.5
120	13.5	27.2	21.7	40.8	120	---	---	---	---	7.3	22.3
130	11.6	25.2	22.0	41.5	130	---	---	---	---	5.3	15.7
140	9.6	23.0	21.2	40.5	140	---	---	---	---	[redacted][a]	(12.5)[a]
150	7.5	20.2	19.2	38.2							
160	6.5	18.0	17.6	35.6							
170	---	---	15.8	32.0							
180(Trig.)	(3.5)[a]	(10)[a]	14.5	26.4							

[a] Estimated values ; [b] From McCombe and Seidel (1967).

The remarkable agreement between the three methods suggests the validity of the Lifshitz-Kosevich theory for Sb and the absence of any non-linear effects, discussed previously in the present experiment. The slight discrepancy between the torque and the field modulation data could be the result of orientation errors. The error is less than 0.5° for the modulation method and about 2° in the torque method.

CHAPTER VI

DISCUSSION OF ALLOYS

1. RIGID BAND MODEL

When a small amount of impurities is added to a pure metal, the rigid band model assumes that no change will occur in the band structure and states that the electron concentration will be raised or lowered by ZCN_o, where Z is the valence difference between host and impurity, C is the atomic concentration of impurities, and N_o is the number of host atoms per cm^3. In terms of Heine's parameter (Heine 1954)

$$R = \frac{A-A_o}{A_o ZC} = \pm \frac{m_o c}{\hbar e} \frac{m_o^*}{F_o D_o(E_F)} \qquad [VI-1]$$

where $A-A_o$ is the change of Fermi surface area from the area A_o of the pure metal, $D_o(E_F)$ is the density of states in the pure metal at the Fermi energy, and F_o and m_o^* are the dHvA frequency and cyclotron mass respectively in the pure metal. If m* is a function of E_F then $(A-A_o)$ is expanded in a Taylor series in E up to second order to give

$$R = \pm \frac{m_o c}{\hbar e} \frac{m_o^*}{F_o D_o(E_F)} \left[\frac{m_o^* + m^*(c)}{2m_o^*}\right] \qquad [VI-2]$$

where $m^*(c)$ is the cyclotron mass of the alloy. The ± signs in [VI-1] and [VI-2] indicate whether the Fermi surface area increases or decreases on alloying. Equation [VI-2] can be

rearranged to give

$$\frac{F-F_o}{F_o} = 1.85\times10^5 \frac{m_o^* ZC}{F_o} \left[\frac{m_o^* + m^*(c)}{2m_o^*}\right] \qquad [VI-3]$$

where a value of $D_o(E_F) = 4.67\times10^{-2}$/atom/eV was used (McCallum and Taylor 1967; Zebouni and Blewer 1967). If $m^*(c) = m_o^*$, Heine's result given in [VI-1] is obtained. The rigid band model can be treated by plotting $\frac{F-F_o}{F_o}$ against the concentration C. A plot of $(F-F_o)/F_o$ vs concentration is shown in Figure 19 where the rigid band prediction of [VI-1] is shown by the solid lines. The dashed lines are the results predicted by the mass dependent R of [VI-3]. The agreement is quite good for the electron and hole branches of Sb-Te alloys.

The change of total carr ier concentration was calculated from the dHvA frequencies using the ellipsoidal approximation. In this approximation, the carrier density of one type is given by

$$n = (8/3\sqrt{\pi})(e/hc)^{3/2}(F_1F_2F_3)^{1/2} p \qquad [VI-4]$$

where p is the number of ellipsoidal pockets, and F_1, F_2, and F_3 are the three principal frequencies. Since the maximum extremal frequencies were not detected experimentally, it was necessary to estimate the carrier concentration n(c) of the alloy by assuming that the relative lengths of the major and minor axes of the Fermi surface remain the same in the alloys. In this case

$$n(c) = (F_c/F_o)^{3/2} n_o \qquad [VI-5]$$

where n_o is the carrier density in pure Sb, and F_c and F_o are the minimum branch frequencies in the alloy and pure Sb respectively. Table 4 shows the total electron and hole carrier densities. The total change of carrier density is compared

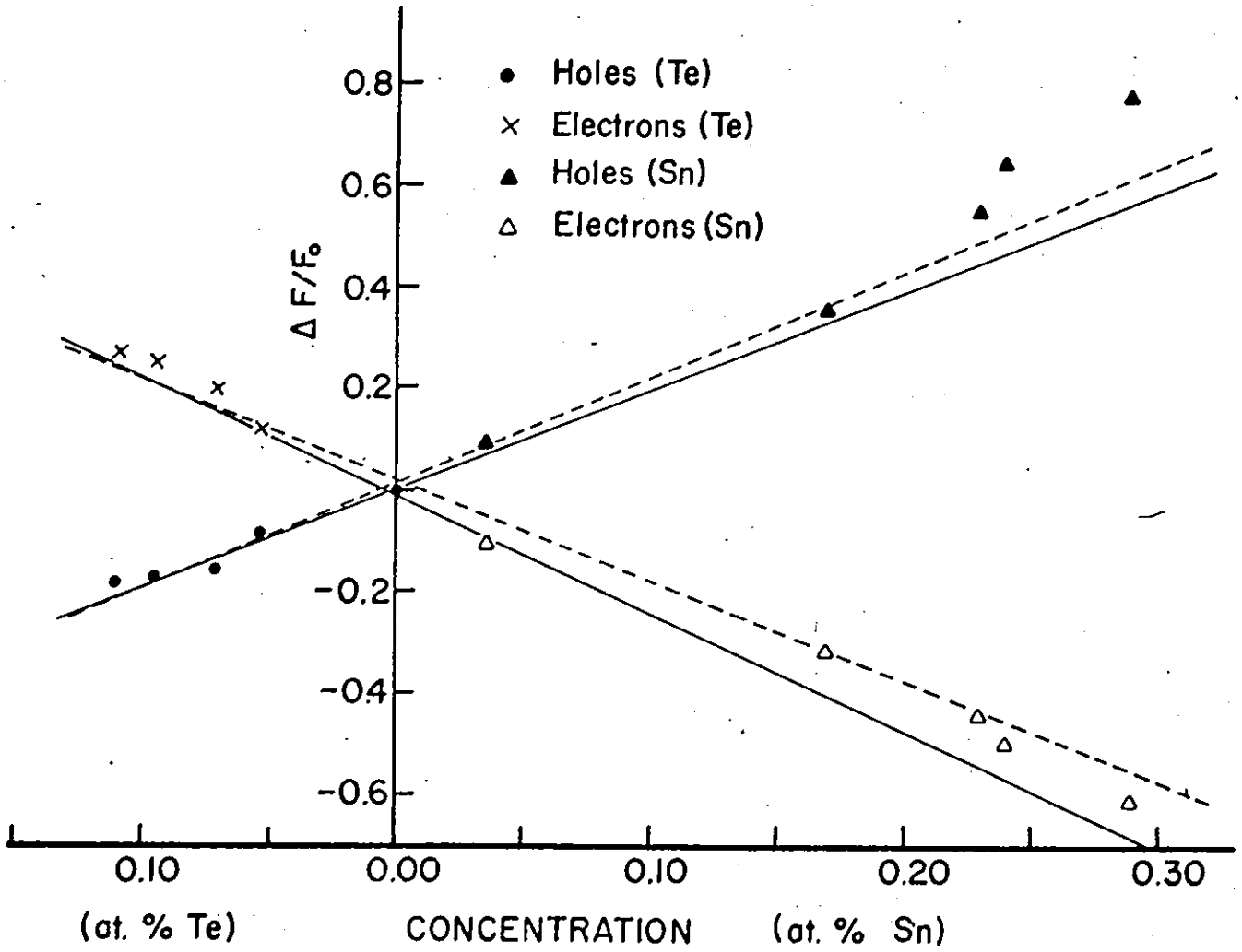

Table 19 Relative frequency shifts at electron and hole minima versus Te and Sn concentrations. The solid lines correspond to the predictions of the rigid band model of [VI-1]. The dashed lines are predicted by the mass dependent model [VI-3].

with the number of Te atoms added. The ratio of the carrier density change to the Te density is shown in the last row. The average value of this ratio is 1.15. The deviation from the rigid

Table 4. Carrier densities in Sb(Te) alloys and change of density from that of pure Sb

Te concentration at. %	0.000	0.054	0.071	0.095	0.110
Number of Te atoms ($cm^{-3} \times 10^{-19}$)	0.00	1.71	2.24	3.01	3.48
Number of electrons ($cm^{-3} \times 10^{-19}$)	5.55	6.53	7.28	7.75	7.89
Number of holes ($cm^{-3} \times 10^{-19}$)	5.52	4.81	4.27	4.12	4.03
Total change of carrier density ($cm^{-3} \times 10^{-19}$)	-	1.69	2.98	3.60	3.83
Total change/no. of Te atoms	-	0.99	1.33	1.19	1.10

band prediction can be attributed to the approximations made in calculating the carrier densities. If the rigid band model holds exactly, the results suggest that the axial ratio for the electron pockets decreases slightly with concentration. The decrease is less than 1% for the highest concentration.

2. BAND SHAPES

In the case of Sb and its alloys it is expected that both hole and electron bands will interact with neighbouring bands having nearly the same energy. The energy surfaces are ellipsoids but the cyclotron masses are energy dependent. This is described by an ellipsoidal, non parabolic energy band of the form

$$E + E^2/E_g = \frac{k_x^2}{m_1} + \frac{k_y^2}{m_2} + \frac{k_z^2}{m_3} \qquad [VI-6]$$

where E_g is the energy gap separating this band from another band near it. The cyclotron mass for an orbit in the xy plane is given by

$$m^* = m_o(1 + 2E/E_g) \qquad [VI-7]$$

where m_o is the band edge mass. The cross-sectional area is

$$A = \pi m_o(1 + E/E_g)E. \qquad [VI-8]$$

Combining [VI-7] and [VI-8]

$$m^{*2} = m_o^2 + (4\pi)(m_o/E_g)A \qquad [VI-9]$$

since A is proportional to the dHvA frequency F,

$$m^{*2} = m_o^2 + .46(m_o/E_g)F \qquad [VI-10]$$

where the value of E_g is in meV, and F is in Tesla. Equation [VI-10] was tested for the electron and hole minima as shown in Figure 20. The data points are reasonably well fitted to a least squares line. The slope of the line gives a value of the $\bar{k}\cdot\bar{p}$ matrix element $E_p (= E_g/m_o)$. The matrix element is 7.1 eV for the holes and 4.8 eV for the electrons. This may be compared to the Sb(Sn) result for which E_p is 7.3 eV for holes and 5.0 eV for electrons. These values compare with 20 eV for III-V semiconductors (Ehrenreich 1961) and 8 eV for Bi(Sb) (Ellett et al. 1966).

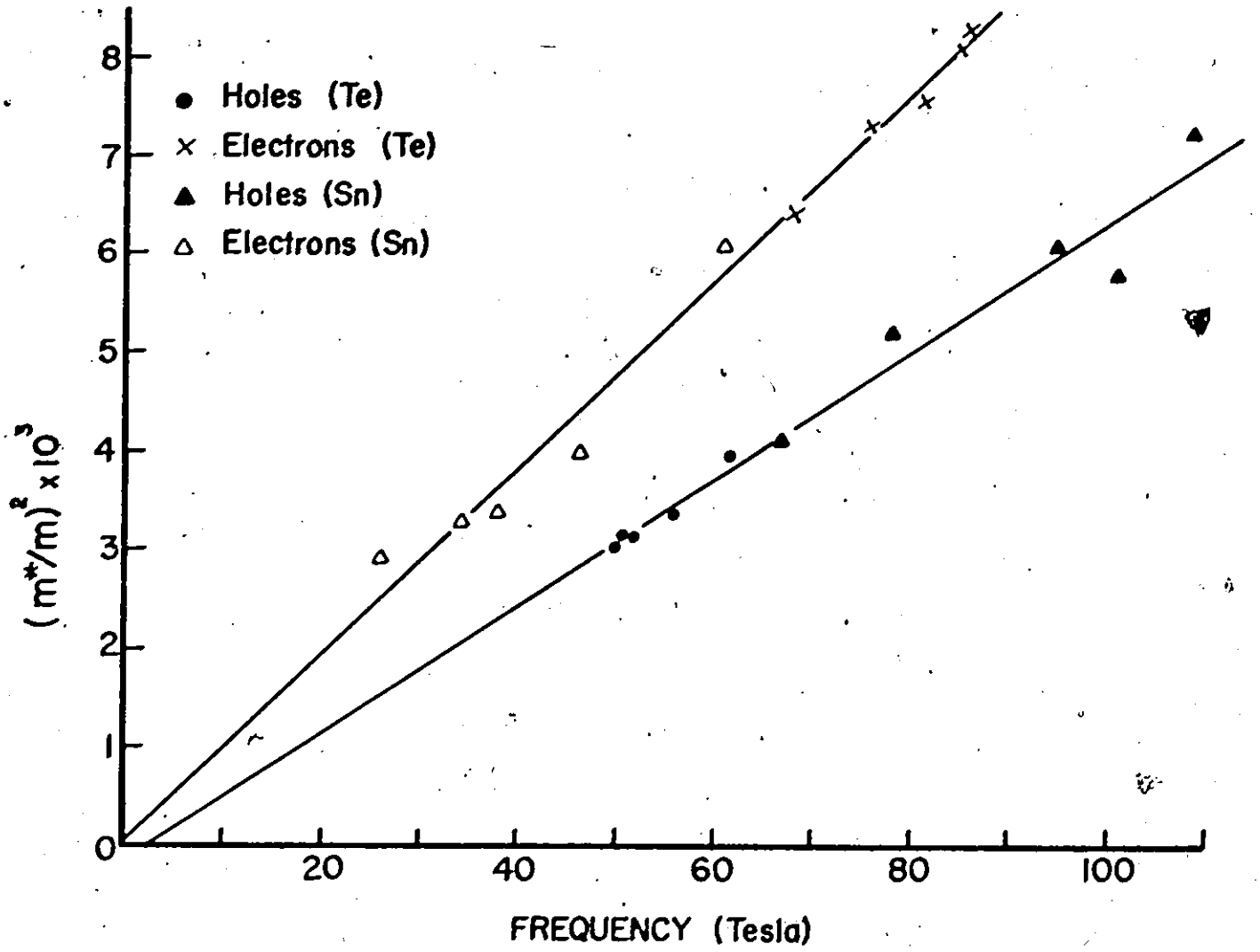

Fig. 20. Square of the cyclotron mass of electrons and holes as a function of dHvA frequency compared with least squares fitted lines predicted by nonparabolic bands.

CHAPTER VII

DISCUSSION OF g-FACTORS

1. THEORY OF THE g-FACTOR IN SOLIDS

In a solid, the g-factor will depart from the free electron value of 2.0023 as a result of spin-orbit interaction and many-body effects. In semimetals and their compounds this departure is almost entirely due to spin-orbit interaction, whereas in the alkali and noble metals the many-body effects arising from the Coulomb interaction between electrons as well as from electron-phonon interactions give the major contribution to the observed g-factors (Randles 1972, Knecht 1975).

The spin-orbit interaction occurs well inside the ion core. The magnitude of the interaction in the solid is then comparable to that of the isolated atom. The g-factors of conduction electrons in solids is determined by the spin-orbit splittings of the valence electrons. The theoretical treatment starts with the one-electron Hamiltonian

$$H = \frac{p^2}{2m} + V(r) + H^{SO} . \qquad \text{[VII-1]}$$

H^{SO} is the spin-orbit Hamiltonian given by

$$H^{SO} = \frac{\hbar^2}{4m^2c^2} \nabla V(r) \times \bar{p} \cdot \bar{\sigma} \qquad \text{[VII-2]}$$

where $\bar{\sigma}$ is the Pauli spin operator and V(r) is an effective potential.

The eigenfunctions are of Bloch form

$$H\psi_{kns} = E_n(k)\psi_{kns} \qquad [VII-3]$$

$$\psi_{kns} = \sqrt{\frac{\Omega}{2\pi^3}}\, e^{i\bar{k}\cdot\bar{r}}\, u_{kns} \qquad [VII-4]$$

where Ω is the volume of the unit cell, the index s, s = 1,2, distinguishes the two spin states and u_{kns} is a periodic two-component function. The problem is usually treated in the effective-mass approximation for the conduction electrons, i.e. one considers only states in the neighbourhood of the energy minimum in the conduction band (n=0, s=1). Measuring $\bar{k}$ from the position of the minimum and for small k (setting $E_o(o) = 0$) the effective-mass Hamiltonian gives

$$E_o(k) = \frac{\hbar^2}{2m}\,\bar{k}\cdot\bar{\alpha}\cdot\bar{k}. \qquad [VII-5]$$

The components of the inverse effective-mass tensor α, can be expressed as (Luttinger and Kohn 1955)

$$\alpha_{ij} = \delta_{ij} + m \sum_{ns} \frac{\langle 01|v_i|ns\rangle\langle ns|v_j|01\rangle + \langle 01|v_j|ns\rangle\langle ns|v_i|01\rangle}{E_o - E_n}. \qquad [VII-6]$$

In the presence of an external magnetic field $\bar{H}$, the one-electron Hamiltonian becomes

$$H = \frac{1}{2m}\left(\bar{P} + \frac{e\bar{A}}{c}\right)^2 + V(r) + \frac{\hbar}{4m^2c^2}\,\bar{\sigma}\cdot\nabla V\times\left(\bar{P} + \frac{e\bar{A}}{c}\right) + \beta\bar{H}\cdot\bar{\sigma} \qquad [VII-7]$$

where $\bar{A}$ is the vector potential and β is the Bohr magneton. In the effective-mass approximation, this Hamiltonian gives

$$\langle Os|H|Os'\rangle = \frac{1}{2m}(\bar{P}_c + \frac{e}{c}\bar{A}_c)\cdot\bar{\alpha}\cdot(\bar{P}_c + \frac{e}{c}\bar{A}_c)\delta_{ss'} - \langle Os|\bar{\mu}|Os'\rangle\cdot\bar{H} \quad [VII-8]$$

where $\bar{P}_c = \hbar k$ is the crystal momentum, and $\bar{A}_c = \frac{1}{2}\bar{H}\times\bar{r}_c$ where $\bar{r}_c = i\hbar\frac{\partial}{\partial P_c}$ is the crystal coordinate operator. The second term in [VII-8] shows that the electron carries with it a magnetic moment

$$\bar{\mu} = \bar{\mu}_\ell + \bar{\mu}_s \quad [VII-9]$$

where

$$\bar{\mu}_s = -\beta\bar{\sigma} \quad [VII-10]$$

and

$$\langle ns|\mu_\ell|ns'\rangle = -\frac{\beta}{\hbar}\langle ns|r\times P|n's'\rangle \quad [VII-11]$$

$\bar{r}$ and $\bar{P}$ are the position and momentum operator respectively.

$$\bar{r}_{ns,n's'}(k) = \frac{2\pi^3}{\Omega}\int u^*_{kns}\, i\frac{\partial}{\partial k}u_{kn's'}d\bar{r} \quad [VII-12]$$

$$\bar{P}_{ns,n's'}(k) = \frac{2\pi^3}{\Omega}\int u^*_{kns}\hbar k\, u_{kn's'}d\bar{r} \quad [VII-13]$$

Using the fact that the periodic functions u_{kns} form a complete set of orthonormal functions $i\frac{\partial}{\partial k}u_{kns}$ may be expressed in terms of u_{kns}. This leads, after some manipulation, to the result (Adams 1952,1953)

$$\bar{r}_{ns;n's'} = \frac{\hbar}{im}\frac{\bar{P}_{ns;n's'}}{(E_{n's'}-E_{ns})} \quad [VII-14]$$

Substituting this result into [VII-11]

$$\langle Os|\mu_\ell|Os'\rangle = -\frac{e\hbar}{2icm}\sum_{ns''}\frac{\langle Os|\bar{P}|ns''\rangle\times\langle ns''|\bar{P}|Os'\rangle}{E_o-E_n} \quad [VII-15]$$

$\langle Os|\bar{\mu}|Os'\rangle$ can be expressed as a linear combination of the unit

matrix and the 3 Pauli matrices, so that

$$- \langle Os|\bar{\mu}|Os'\rangle \bar{H} = \frac{1}{2} \beta \sum_{ij} G_{ij} H_i \sigma_j \qquad \text{[VII-16]}$$

has the eigenvalues

$$E = \pm \frac{1}{2} g\beta H \qquad \text{[VII-17]}$$

with the effective g-factor given by

$$g = \left[\sum_{ij\ell} \lambda_i \lambda_j G_{i\ell} G_{j\ell} \right]^{1/2} \qquad \text{[VII-18]}$$

where λ_i are the direction cosines of $\bar{H}$ with respect to the coordinate axes. The quantity $Q_{ij} = \sum_{\ell} G_{i\ell} G_{j\ell}$ is a second rank symmetric tensor and can be diagonalized. If its principal components are g_i^2 and λ_i' are the direction cosines of $\bar{H}$ with respect to the principal axes of Q_{ij}, then

$$g = \left[\lambda_1'^2 g_1^2 + \lambda_2'^2 g_2^2 + \lambda_3'^2 g_3^2 \right]^{1/2} . \qquad \text{[VII-19]}$$

From the g-factor, one can define a spin-mass, m_s, (Cohen and Blount 1960)

$$\frac{m_s}{m_o} = \frac{2}{g} . \qquad \text{[VII-20]}$$

The occurrence of small energy gaps points to small spin masses or large g-factors. This is because $\bar{\mu}_\ell$ can become very large when there is a small gap since $\bar{r}$ is proportional to the reciprocal of a gap (see [VII-14]). This orbital magnetic moment, $\bar{\mu}_\ell$, arises from interatomic circulating currents, in other words, from electron orbits extended over

several atomic sites. To obtain an estimate of g-factors in the presence of strong spin-orbit coupling, one can write $e\delta v$ for the circulating current, where δv is the spread in the orbital velocity which is given by the uncertainty principle $m^*\delta v\delta x = \hbar$, the orbital moment is $\mu_\ell = \frac{e}{2c}\delta x\delta v = \frac{e\hbar}{2m^*c}$ giving a g-factor of $\frac{2m_o}{m^*}$ which is large when m^* is small.

2. APPLICATION TO ANTIMONY

The k=0 conduction band for electrons is at the point L in the Brillouin zone which is a mirror plane and possesses inversion symmetry (2/m). The Fermi surface is nearly ellipsoidal with a center of symmetry and the calculation of g-factors can be carried out using the method of Cohen and Blount (1960) for bismuth. For the holes, however, the k=0 conduction band does not possess inversion symmetry and one cannot use this method.

The valence band closest to the conduction band is considered. This one level approximation is valid when the gap, E_g, between the conduction and valence bands is small compared to the spin-orbit energy Δ. This means that only this single level contributes to the α_{ij} and μ_ℓ. This is true if all the α_{ii} are large. From the cyclotron mass data of Datars and Vanderkooy (1964) one obtains the following values of the electron α_{ij}

$$\alpha_{xx} = 10.75$$

$$\alpha_{yy} = .93$$

$$\alpha_{zz} = 11.5$$

$$\alpha_{yz} = .835$$

$$\alpha_{xy} = \alpha_{xz} = 0$$

where x, y, and z stand for the binary, bisectrix and trigonal directions. The small value of α_{yy} indicates the existence of another nearby valence band contributing to the spin-orbit interaction. Thus, the method of Cohen and Blount is valid only at orientations where α_{yy} does not contribute to μ_ℓ and hence the g-factor. This is true for such planes that contain the bisectrix axis. Therefore, the calculations will be done only for the trigonal-bisectrix plane.

The method of Cohen and Blount for Bi is followed with two modifications. Firstly, as the α_{ij} for Sb are much smaller than in Bi, the δ_{ij}'s in [VII-6] are not neglected. Similarly, in the calculations of μ, the spin magnetic moment μ_s is not ignored. Secondly, both spin-split valence band states $|a1\rangle$ and $|a2\rangle$ are considered at energies E_g and $E_g+\Delta$ from the conduction band $|01\rangle$, i.e. the problem is treated in the two-level approximation. The g-factor in the trigonal-bisectrix plane from Equation [VII-18] is

$$g = [\lambda_z^2(G_{zz}^2+G_{zy}^2+G_{zx}^2) + \lambda_z\lambda_y(G_{zz}G_{yz}+G_{zy}G_{yy}+G_{zx}G_{yx}) + \lambda_y^2(G_{yy}^2+G_{yz}^2+G_{yx}^2)]^{1/2} . \qquad [VII-21]$$

The G_{ij}'s are calculated from [VII-15] and [VII-16]. From group theoretical considerations, the only non-vanishing velocity

matrix elements that enter [VII-15] are (Cohen and Blount 1960)

$$\langle 01|V_x|a2\rangle, \quad \langle 01|V_y|a1\rangle, \text{ and } \langle 01|V_z|a1\rangle$$

which in turn can be expressed in terms of α_{ij} using [VII-6]. The results are

$$g_y=[\tfrac{1}{2}|(\alpha_{zz}-1)(\alpha_{xx}-1)|f^2 + \sqrt{|(\alpha_{zz}-1)(\alpha_{xx}-1)|}\, f+A]^{1/2} \quad \text{[VII-22]}$$

$$g_z = [\tfrac{1}{2}|(\alpha_{xx}-1)(\alpha_{yy}-1)|f^2 + 4]^{1/2} \quad \text{[VII-23]}$$

where

$$f = [\frac{E_g+\Delta}{E_g} + \frac{E_g}{E_g+\Delta}]^{1/2} .$$

In Sb the valence band is the 5p level. Thus it has the same electronic configuration as Sb III. The 5p level splits into $p_{1/2}$ and $p_{3/2}$ levels with an atomic spin-orbit splitting of .81 ev. (Lang 1930, Kane 1957). For non-cubic crystals, for example orthorhombic, the splitting is 2/3 of the corresponding cubic structure (Falicov and Golin 1965). The renormalization factor for the spherical (atomic) to cubic systems can be easily found from the known spin-orbit splitting of a material having identical electronic configuration . In the case of Sb III, this material is Sn II for which Δ(atomic) = .525 eV. (Lang 1930) and Δ(solid) = .48 eV (Cardona et al. 1967). The spin-orbit splitting, Δ, for Sb is then

$$\Delta = .81 \times \frac{2}{3} \times \frac{.48}{.525} = .49 \text{ eV.}$$

The energy gap, E_g, for Sb determined from the magneto-

reflection experiments of Dresselhaus and Mavroides (1965) is .10 eV. Using these values for Δ and E_g, Equation [VII-21] becomes:

$$g = \{7.62 \cos^2(180-\theta)+34.8 \cos(180-\theta)\cos(90-\theta)+313 \cos^2(90-\theta)\}^{1/2} \quad [VII-24]$$

where the angle θ is measured from the trigonal axis in the same sense as in Fig. 9. The g-values calculated from Equation [VII-24] are plotted together with the lower set of g-values, determined from the field modulation experiments so as to minimize errors due to crystal misorientation, in Fig. 21. It is clear that the agreement is very good with this choice of g-values. It should be mentioned that Equations [VII-22], [VII-23] and [VII-24] reproduce the result of Cohen and Blount $m_s = m^*$, also shown for comparison purposes in Fig. 16, if one neglects the contributions of the spin-split bands $|02\rangle$ and $|a2\rangle$. i.e. by putting $\Delta=0$ and multiplying the result of the g-factors by 2 since now the pair of levels $|01\rangle$, $|02\rangle$ and $|a1\rangle$, $|a2\rangle$ are identical.

3. COMPARISON WITH SPIN RESONANCE DATA

Spin resonance experiments yield values of the spin mass and provide additional evidence for resolving the existing ambiguity in the g-factor determined from dHvA experiments. This comparison is particularly important for cases where no theoretical calculations could be performed, as in the case for the antimony hole Fermi surface. Before discussing spin reso-

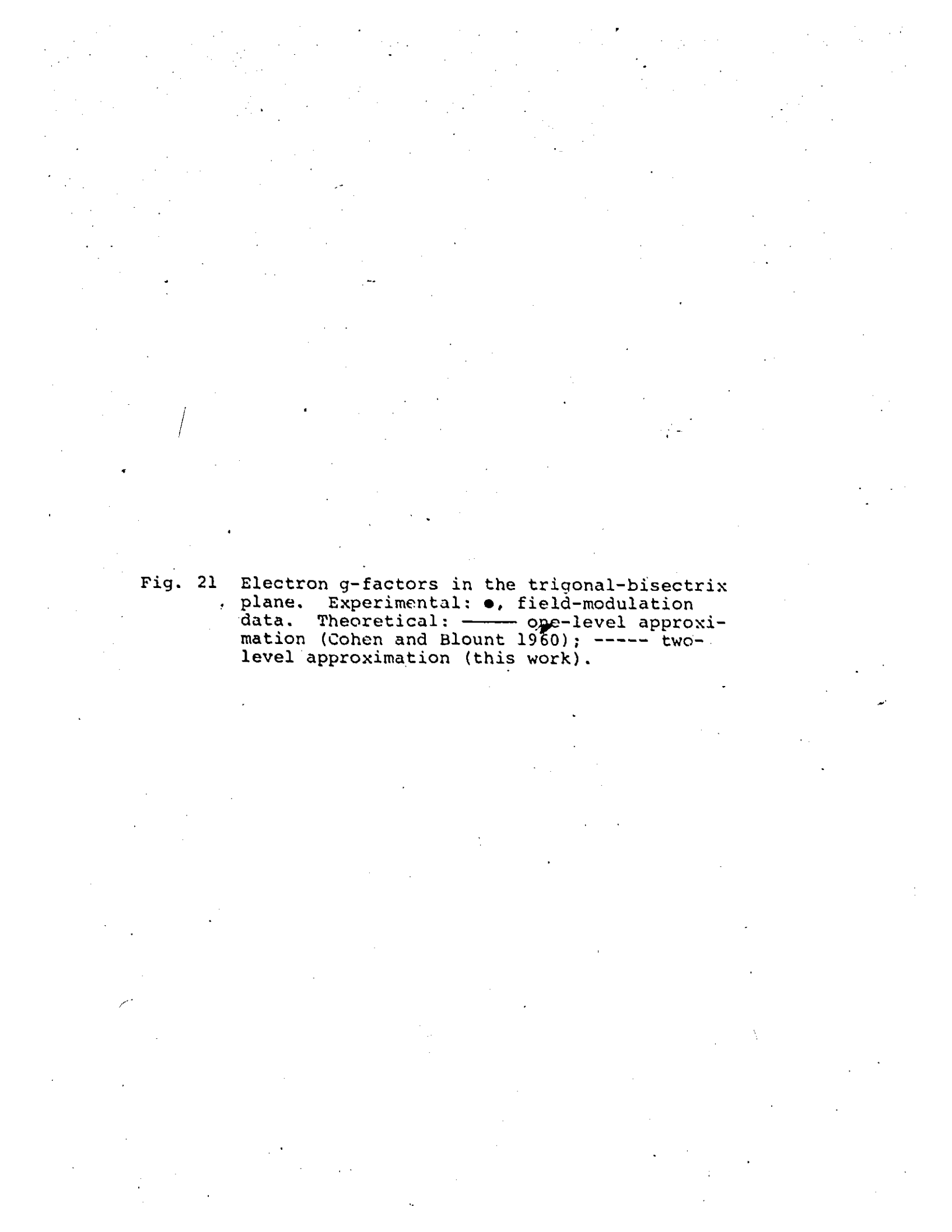

Fig. 21 Electron g-factors in the trigonal-bisectrix plane. Experimental: ●, field-modulation data. Theoretical: ——— one-level approximation (Cohen and Blount 1960); ----- two-level approximation (this work).

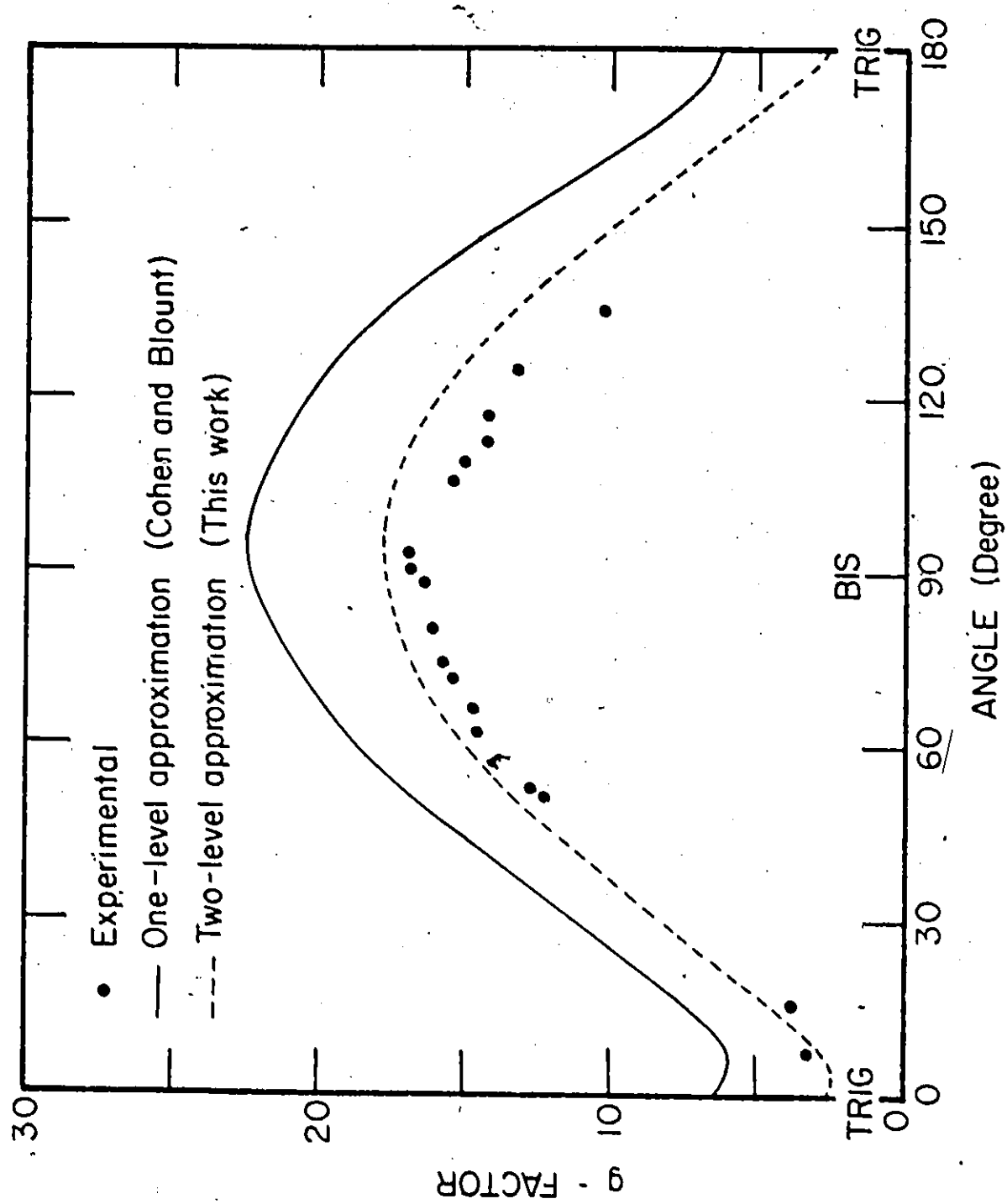
• Experimental
— One-level approximation (Cohen and Blount)
--- Two-level approximation (This work)
g - FACTOR
30
20
10
0
TRIG
0
30
60
BIS
90
120
150
180
TRIG
ANGLE (Degree)

nance experiments, it is beneficial to present a physical picture of the existing ambiguity. For antimony, the higher and lower g-factor branches shown in Fig. 21 correspond to the effective mass m* being larger or smaller than the spin mass m_s, respectively. The energy level diagram for a few Landau levels including spin-splitting is shown for the two cases in Fig. 22. It is evident that for a dHvA-type experiment the two cases are identical, so that there is an ambiguity. In a resonance experiment, on the other hand, transitions of type 1,2,3 and 4 are expected to occur. Type-1 transitions are just cyclotron resonance transitions taking place between successive Landau levels having the same spin state. Type-2 transitions are pure spin-resonance, while type-3 and 4 transitions involve both an orbital and a spin transition. It is clear from Fig. 22 that only transitions of type 2 and 4 can discriminate between the two cases. Extensive spin resonance experiments on Sb were done by Datars (1962). The sign of carriers and details of the Fermi surface were not yet determined, so that some readjustments were necessary in interpreting the spin resonance data. At a general field direction up to five cyclotron mass branches may coexist which make assignments of spin resonance data rather difficult. Thus comparisons will be made only at the two symmetry directions.

For the magnetic field parallel to the trigonal axis the observed type-4 transition gives an effective mass, m_4, of .057 m_o for holes. From the energy level diagram $E_4 = E_2 + E_1$

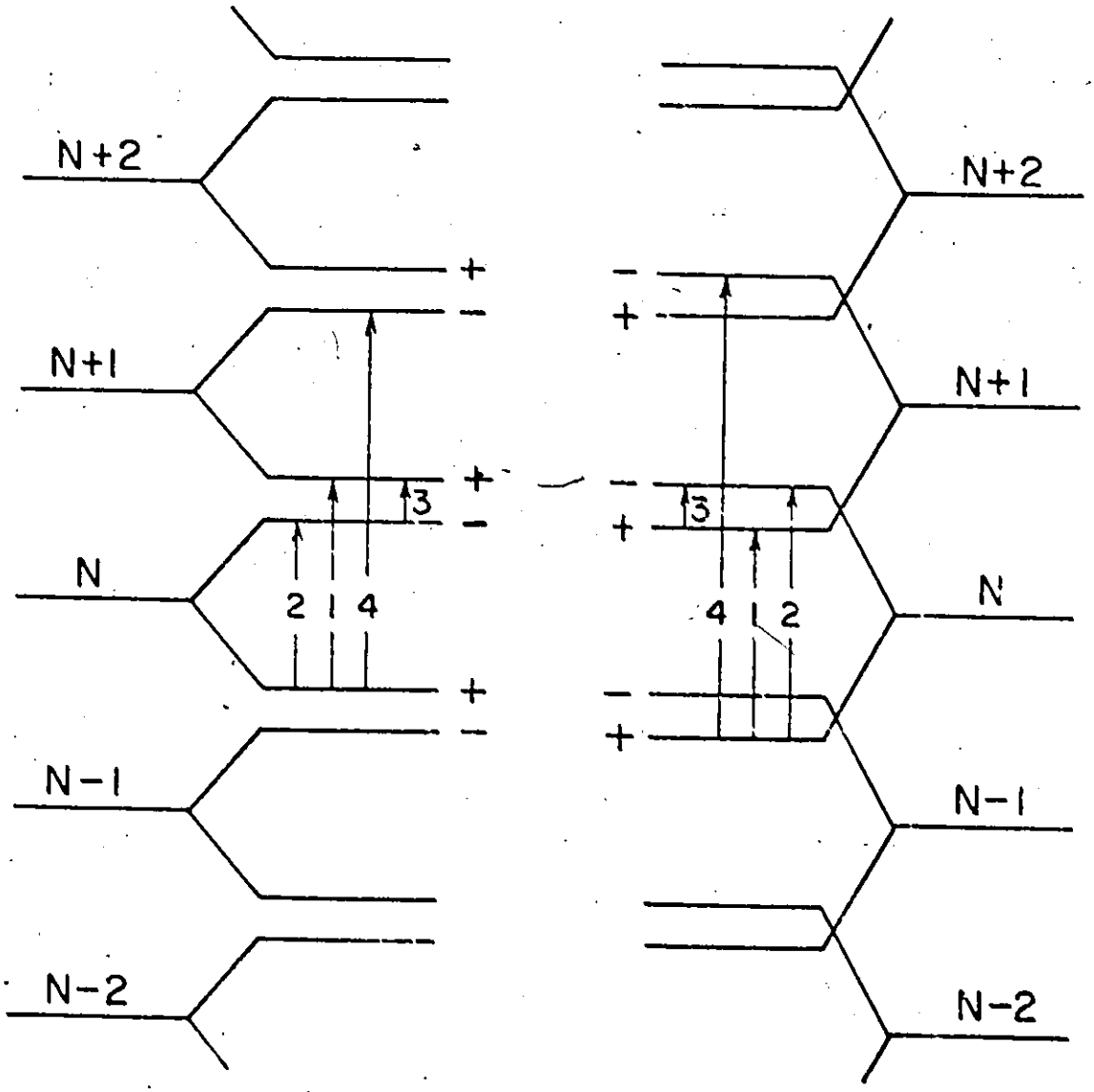

Fig. 22 Possible transitions between spin-split Landau levels for $m^* < m_s$ (Case I) and $m^* > m_s$ (Case II).

or equivalently

$$\frac{1}{m_4} = \frac{1}{m_s} + \frac{1}{m^*} \qquad \text{[VII-25]}$$

and using the value of the effective mass at the trigonal direction [VII-25] is solved for m_s. The resulting g-factor is 15.0 in excellent agreement with the lower branch g-factor value of 14.5 corresponding to case I of Fig. 22. Moreover, the transition observed at 8.1 kOe is an electron type-2 transition giving a g-factor of 3.0 also in good agreement with both the observed (lower branch) and the calculated g-factor.

At the binary direction, the observed type 4 transition gives an effective mass, m_4, of .0452 m_o for the non-principal hole branch. Using [VII-25] the spin mass is found to be .123 m_o or a g-factor of 16.3. The lower branch g-factor value for the non-principal holes is 16.5. In addition to the type-4 transition, the type-2 transition observed yields a spin value of .63 m_o or a g-factor of 3.2 for the principal hole branch. The corresponding experimental value is about 4 for case I. Thus the spin resonance results show that the lower set of g-factor values for holes should be used.

Finally, the small discrepancy between theory and experiment (Fig. 21) may be due to an overestimation of Λ, the influence of a third energy level and/or many body effects. Since the magnitudes of these effects are not known at the present time, one cannot draw any conclusions about the contribution of many body effects on the g-factor of Sb.

CHAPTER VIII

CONCLUSIONS

The dHvA frequencies, cyclotron masses, and Dingle temperatures of Sb(Te) alloys with up to 0.11 at.% Te were measured. In the concentration range of study, the electron and hole frequencies increased and decreased, respectively, as the concentration of Te was increased. These changes are well accounted for by the rigid band theory. Figures 8 and 19 summarize the change of cyclotron mass and dHvA frequency with concentration of Sn and Te. The change in mass for both alloy systems is explained by nonparabolic energy bands. The change in frequency is explained by a mass dependent rigid-band model except for the holes with high tin concentration. The results of Sb(Te) and Sb(Sn) show the validity of the rigid band model for impurities with a valence difference of one. This confirms the predictions about alloying made by Stern (1972).

The change in cyclotron mass with concentration gives direct indication of the nonparabolic nature of the bands. The difference in the rate of mass change of electrons and holes further suggests different band shapes for the two carriers. An ellipsoidal-nonparabolic band gives a good fit for the cyclo-

tron mass data. The $\bar{k}\cdot\bar{p}$ matrix element is 7.1 eV for holes and 4.8 eV for electrons.

Estimates of the Fermi surface volume indicate that each Te atom contributes a conduction electron to the alloy.

The g-factors for electrons and holes were deduced from the harmonic content in the oscillation waveform obtained by the torque and field modulation techniques. Direct observations of spin-splittings at sufficiently high magnetic fields in the torque method provided an independent measurement of the g-factors. The excellent agreement between these three methods suggests the validity of the Lifshitz-Kosevich equation for antimony and the absence of non-linear effects. Infinite field phase measurements on electrons and holes indicate that the spin-splitting terms are negative for both carriers. This reduced the number of g-factors that are reasonable to just two. A theoretical g-factor calculation in the effective mass approximation for the conduction electrons, which possess inversion symmetry, was carried out. The theoretical treatment is based on the method of Cohen and Blount (1960) for bismuth. However as the spin-orbit gap in antimony is smaller than that of bismuth the calculations were done in the two-level approximation. The results are in excellent agreement with the lower set of electron g-factor values. These results are also in good agreement with electron spin resonance data (Datars 1962). Spin resonance data for holes also indicate that the lower set of

the hole g-factors is the correct one. The g-factors at the binary, bisectrix and trigonal directions are found to be ~15, 16.8, 3.5 and 4.5, 18.0, 14.5 for the principal branches of electrons and holes respectively.

BIBLIOGRAPHY

Adams II, E.N. 1952. Phys. Rev. 85, 41.

Adams II, E.N. 1953. J. Chem. Phys. 21, 2013.

'Abrikosov, N. Kh., Poretskaya, L.V., and Ivanova, I.P. 1959. Zh. Neorg. Khim. 4, 2525; (Engl. Transl.; Russ. J. Inorg. Chem. 1959. 4, 1163).

Alles, H. and Lowndes, D.H. 1973. Phys. Rev. B, 8, 5462.

Alles, H., Higgins, R.J., and Lowndes, D.H. 1975. Phys. Rev. B,12, 1304.

Bhargava, R.N. 1967. Phys. Rev. 156, 785.

Braun, I. and Wang, E.Y. 1961. Solid-State Electron. 3, 79.

Bresler, M.S. and Red'ko, N.A. 1972. Soviet Phys. J.E.T.P. 34, 149.

Rychkov, Yu. A. and Gor'kov, L.P. 1962. Soviet Phys. J.E.T.P. 14, 1132.

Cardona, M., Shakleo, K.L., and Pollack, F.H. 1967. Phys. Rev. 154, 696.

Cohen, M.H. and Blount, E.I. 1960. Phil. Mag. 5, 115.

Coleridge, P.T. and Templeton, I.M. 1971. Can. J. Phys. 49, 2449.

Coleridge, P.T. and Templeton, I.M. 1972. J. Phys. F:Metal Phys. 2, 643.

Datars, W.R. 1962. Phys. Rev. 126, 975.

Datars, W.R. and Vanderkooy, J. 1964. I.B.M. J. of Res. and Devel. 8, 247.

Dresselhaus, M.S. and Mavroides, J.G. 1965. Phys. Rev. Letters 14, 259.

Dunsworth, A.E. and Datars, W.R. 1973. Phys. Rev. B, 7, 3435.

Ehrenreich, H. 1961. J. Appl. Phys. (Suppl.) 32, 2155.

Ellett, M.R., Horst, R.B., Williams, L.R., and Cuff, K.F. 1966. J. Phys. Soc. Jap. 21, Suppl. 666.

Falicov, L.M. and Golin, S. 1965. Phys. Rev. 137, A871.

Falicov, L.M. and Lin, P.J. 1966. Phys. Rev. 141, 562.

Goldstein, A., Williamson, S.J.W., and Foner, S. 1965. Rev. Sci. Instr. 36, 1356.

Heine, V. 1954. Proc. Phys. Soc. Lond. A, 69, 505.

Herod, R.D., Gage, C.A., and Goodrich, R.G. 1971. Phys. Rev. V, 4, 1033.

Hornfeldt, S., Ketterson, J.B., and Windmiller, L.R. 1973. J. Phys. E: Sci. Instrum. 6, 265.

Ishizawa, Y. 1968. J. Phys. Soc. Jap. 25, 150.

Kane, E.O. 1967. J. Phys. Chem. Solids 1, 249.

Kao, Y.H. 1964. Phys. Rev. 136, A858.

Knecht, B. 1975. to be published.

Landau, L. 1956. Soviet Phys. J.E.T.P. 3, 920.

Lang, R.J. 1930. Phys. Rev. 35, 445.

Lifshitz, I.M. and Kosevich, A.M. 1956. Soviet Phys. J.E.T.P. 2, 636.

Luttinger, J.M. 1956. Phys. Rev. 102, 1030.

Luttinger, J.M. and Kohn, W. 1955. Phys. Rev. 97, 869.

McCallum, D.C. and Taylor, W.A. 1967. Phys. Rev. 156, 782.

McCombe, B. and Seidel, G. 1967. Phys. Rev. 155, 633.

Nanney, C. 1963. Phys. Rev. 129, 109.

Onsager, L. 1952. Phil. Mag. 43, 1006.

Phillips, R.A. and Gold, A.V. 1969. Phys. Rev. 178, 932.

Poulsen, R.G., Moss, J.S., and Datars, W.R. 1971. Phys. Rev. B, 3, 3107.

Randles, D.L. 1972. Proc. R. Soc. Lond. A, 331, 85.

Shoenberg, D. and Vuillemin, J.J. 1966. Proc. L.T. 10, Moscow, 3, 67.

Stark, R.W. and Falicov, L.M. 1967. Progress in Low Temp. Physics 5, 235.

Stern, E.A. 1972. Proceedings of the Michigan State University Summer School on Alloys (Michigan State University, Ann Arbor, Mich.)

Tanaka, K., Suri, S.K., and Jain, A.L. 1968. Phys. Rev. 170, 664.

Vanderkooy, J. and Datars, W.R. 1968. Can. J. Phys. 46, 1215.

Weiner, D. 1962. Phys. Rev. 125, 1226.

Windmiller, L.R. 1966. Phys.Rev. 149, 472.

Windmiller, L.R. 1973. Mont Tremblant International Summer School on Transition Metals, Alloys and Magnetism (Mont Tremblant, Quebec).

Yafet, Y. 1952. Phys. Rev. 85, 478.

Yafet, Y. 1957. Phys. Rev. 106, 679.

Zebouni, N.H. and Blewer, R.S. 1967. Phys. Lett. A, 24, 106.